Analysis of Wireless Communication over Electromagnetic Impulse Noise Channel

Akash Kumar Mandal and Swades De

Abstract

Wireless communication in power grid environment faces peculiar power system environment specific noise. Owing to its impulsive nature, the characterization of such noise is critically important and fundamentally different from the existing analysis. This paper presents a theoretical analysis of the impact of power system electromagnetic impulse noise in smart grid environment on the performance of wireless communication between the grid health monitoring devices (e.g., Phasor Measurement Units) and the local data concentrator. It uses a classical approach in the derivation of a re-parameterized impulse noise model from its characteristic function. A comparison of outage probability between the corona impulse noise (CIN)-ridden and noise-free channel is studied. The study is extended for comparison with co-channel interference (CCI) for establishing a better understanding of the power specific electromagnetic impulse noise. A modified performance metric called signal-to-pulse-noise ratio is defined and its probability distribution is derived and compared with the additive white Gaussian noise, CIN and CCI-ridden channel statistics. The physical layer wireless channel characterization analysis is extended further to study the average system throughput via Markov modeling of the channel.

Index Terms

Communication in smart grid environments, corona impulse noise, co-channel interference, signal-to-pulse-noise ratio, CuRD index, Markov analysis, throughput

I. Introduction

With the growth in power system dimensions owing to higher demands and rising industrialization, power system ailments have also increased manifold. To ensure power supply reliability, the system limitations need to be adequately addressed. It is even better if the critical occurrences

The authors are with the Department of Electrical Engineering and Bharti School of Telecommunication, Indian Institute of Technology Delhi, New Delhi 110016, India.

could be predicted for prevention. Incorporation of smart and semi-smart Internet of Things (IoT) devices, such as smart meters, digital relays, and phasor measurement units (PMUs) has offered a boost to this motive. It has been amply demonstrated in literature that the IoT data can be used to prevent and arrest many critical power system faults [1], [2]. The PMU data, such as powerline phasor voltage, current, frequency and its rate of change can be used to remotely monitor and possibly control the power system health in real time via phasor data concentrators (PDCs). Therefore correct reception of the data is very important [3].

Considering these grid monitoring devices as nodes, communication to a base station could be either wired or wireless. Wireline communication is neither cost effective nor convenient. Wireless connectivity for smart grid IoT communication is a promising alternative. However, unlike the conventional wireless environment, wireless communication in power grid environments is expected to face hurdles of more complicated electromagnetic noise (EMN). The channel disturbance generated from the various electromagnetic sources would affect the system performance in a more intricate fashion [4], which could have severe impact on dynamic grid health monitoring. Also, an increased demand for data rates is of prime importance, especially from the viewpoint of power system protection and monitoring, which calls for higher spectral usage in current as well as future smart grid wireless communication networks.

In high voltage transmission scenarios such as in power grid environments, blue discharge is caused by air ionization around the conductor, generating an EMN, called 'corona discharge'. The data in [5] has validated that the corona noise power at a receiver 1 m away from the corona impulse source (CIS) can be as high as -5 dBm at 1000 MHz. Using the Friis free space equation, the minimum power at a receiver placed 1000 m from the corona noise source can be calculated approximately to be -95 dBm. Again, using the Friis equation at constant transmit power P_{Tx}, transmitter gain G_{Tx}, receiver gain G_{Rx} and transmitter-receiver distance R we have,

$$P_{r,2}[dB] = P_{r,1}[dB] + 20\log\left(f_1/f_2\right) \tag{1}$$

where $P_{r,1}$ and $P_{r,2}$ are received power at the antenna under all the mentioned constants for wavelengths $1/f_1$ and $1/f_2$ respectively. From (1) it can be calculated that, at 2.4 GHz corona noise spans over a bandwidth of 2 GHz with ≈ -100 dBm strength, which is comparable to or stronger than the receiver thermal noise (≈ -114 dBm) [5], [6]. The impact and existence

of corona noise on powerline communication is analyzed in [7]. Further, the pervasive presence of such noise can be established from the measurements presented in [3], [8] where the later discusses its presence over a wider band of line voltage ranging from 2.4-800 kV. Therefore, for a better understanding of wireless communication performance in smart grid environment, it is important to mathematically characterize the effect of such noise. Moreover, because of impulsive nature of corona noise, analysis using the average values of the noises is not practical or realistic in such dynamic environments with electromagnetic radiations.

The aim of this paper is to investigate the impact of power system electromagnetic corona noise on the wireless data communication between any two smart grid IoT nodes involved in grid health monitoring. Therefore, PMU-to-local PDC communication serves as a practical use case owing to its strict measurement and processing latency constraints.

A. Literature Review and Motivation

The work thus far can be broadly put in three sets. In the first set [9], [10], [11], [12], statistical analysis of generic impulse noise was of interest. Most of the grid-specific noise modelings were in the context of powerline communication which is not useful for wireless communication [13], [14]. Also, none of the existing attempts captures the exact nature of power system corona noise owing to two basic shortcomings: (1) spatio-temporal variation of corona impulse sources, and (2) infinite impulse emissions per source in practical settings. Both these factors are probabilistic and could be parameterized on line voltage, atmospheric conditions, and conductor spacing. Also, not all corona noises have the same EMN impact over a frequency band of interest. For example, EMN from positive corona noises, such as onset pulses, Hermstein's glow, and positive streamers, decay much faster than their negative counterparts, such as Trichel pulses, pulseless glows, and negative streamers. Hence, a window-dependant statistical characterization is important.

The second set considered the study of power system impulsive noise through experimental set-ups and the conditions affecting its generation and impact on the electrical power systems. The studies in [15], [16], [17] performed the time characterization of corona noise on high voltage transmission lines. Similarly, the work in [5], [18] corroborate the impact of power system corona noise on smart grid wireless communication through an experimental study, but they do not capture the performance via mathematical analysis. The work in [19] studied the impulsive nature of corona noise in a similar environment. All these studies analyzed either the existence of corona noise or its impact on the power delivery through transmission and

distribution lines; the communication aspect stayed untouched. However, they clearly indicate that these power specific noises have a strong impact on the communication system. These set of studies motivate the need for a mathematical analysis of corona impulse noise (CIN) in the context of data communication.

The last set of works [20], [21] aimed at filling the analysis gap by determining the system parameters for wireless communication under impulsive noise, which has also been discussed in [22] for smart grid applications. These works however used the average signal-to-interference-noise ratio (SINR) expressions [23], which do not capture the communication system performance well in power system's asynchronous noise environment. This is because of highly impulsive nature of CIN. Therefore, it is very important to find a closed-form distribution of instantaneous SINR in such scenarios [24]. This helps in understanding the instantaneous channel characteristics and consequently in channel-adaptive data transmission. Moreover, even the time averaged analysis of power system impulsive noise has not yet been considered to establish a comparative study of such smart grid EMN on wireless communication.

Powerline communication has been studied in much depth in the recent past, but similar analysis and modeling for the wireless communication is yet to be studied well. The work in [25] mentions the severity and uniqueness of the smart grid environment for wireless communication, however it does not analyze the impact. Similarly, the work in [6] deals with power system impulsive noise modeling, but from the perspective of powerline communication. Although this work establishes the inadequacy of the existing probabilistic models in the characterization of impulsive noise, it does not develop any appropriate model for such noises. The work in [26] and [27] demonstrated experimentally the impact of EMN on the wireless data relay and proved that under certain practical adversities the bit error rate (BER) could be as high as 100%. They conducted experimental analysis of the EMN spectrum from 70 kV, 110 kV, and 400 kV electric transmission lines between $10-30$ MHz, and thus laid an even stronger need for mathematical modeling of such an EMN environment and study its impact on the communication performance.

Apart from surrounding wireless channel conditions, corona noise generation is dependant on powerline design and voltage gradient between lines and air, which is supported by the design manual in [28], and can not be captured by any external measuring device.

B. Contribution and Significance

This work focuses on analyzing wireless communication in power grid environment, devising exact expressions on the relevant performance parameters, and presenting a comparative study with different known communication scenarios. The key contributions are as follows:

1) Power system specific modeling of the re-parameterized impulse noise and co-channel interference is conducted, considering a space-time varying number of corona noise sources.
2) A power system specific power ratio parameter called signal-to-pulse-noise ratio (SPNR) specific to impulsive noises is defined and exact expressions for total unwanted power, receiver SPNR and outage probability are derived for single-user as well as multi-user communication scenarios. A new parameter called cumulative relative dispersion (CuRD) index is defined which captures the EMN characteristics.
3) Throughput performance is mathematically analyzed and the impact of EMN from powerlines on wireless communication is quantified. Using the concepts of level crossing rate (LCR) and average fade duration (AFD) a Markov model is developed for analytically capturing the average throughput performance in power grid environments.

The simulation results reveal that the power system environment has a strong adverse effect on wireless communication. Hence, channel characterization of such communication environments is important. The study in this paper is important in quantitatively understanding the impact of electromagnetic impairments that the powerlines can cause to wireless communication. It also provides valuable insights on the control strategies that could be incorporated in such scenarios.

C. Paper Organization

The paper layout is as follows. Section II presents the system model. Section III contains the power system specific modeling of co-channel interference (CCI) and CIN. exact expressions of total unwanted power and SPNR leading to the expression for outage probability are derived in Section IV. Average throughput analysis is done in Section V. Simulation results are discussed in Section VI, followed by the concluding remarks in Section VII.

II. System Model for Smart Grid Wireless Communication

Fig. 1 illustrates the background power system environment and the proposed system model used in the analysis. The inter-PMU communication and the communication between PMU

and the local phasor data concentrator (PDC) are considered to be over wireless medium. The PMUs exchange real-time data amongst themselves, and with a local PDC for power system grid monitoring, fault prediction, and protection in an electromagnetic environment. As discussed before, one of the prominent EMNs is corona noise. These corona noise pulses can be of varied types which will be dealt in depth in the next section during the statistical modeling. A scenario is analyzed with these devices communicating through Wi-Fi protocol, where the loss of data could be critical leading to impaired grid details or loss of grid health data. This system model considers randomly varying CISs in PMU$-$PDC communication, which are located at different points in the grid leading to time varying impulse noise effects. The high voltage units namely generation, transmission and heavy load distribution sides generate CISs. They are locally monitored and controlled by their local data collectors, which send the data further to a central data center for complete grid monitoring. Let A_c be the total number of corona noise sources and B_{α_c} be the number of active impulse from the α_c-th source in the window of interest.

Every corona impulse can be parameterized on two important statistical terms, τ_{α_c,β_c} (the reference duration of β_c-th impulse from α_c-th source referenced at $t = 0$) and T_{α_c,β_c} (the duration of each impulse). This is a valid assumption because the corona noise is highly impulsive. The inter-arrival times ($\Delta\tau_{\alpha_c,\beta_c}$) of corona impulses is exponentially distributed. Also, the occurrence

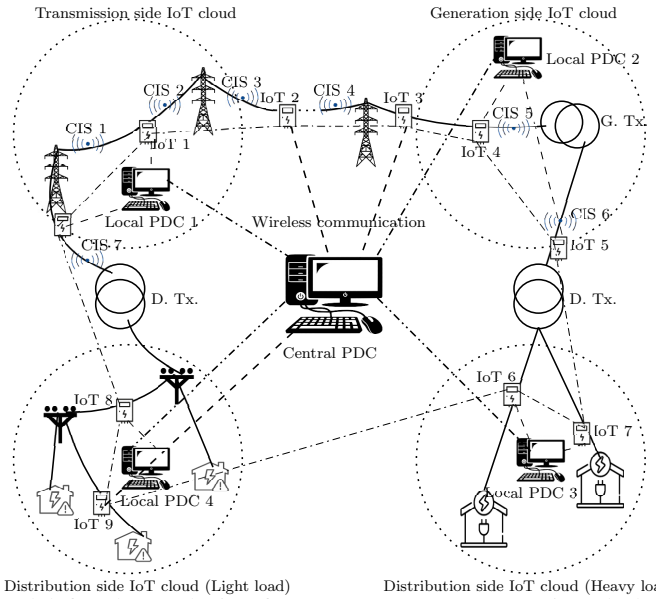

Fig. 1: Wireless system model for the analysis of power system corona noise. dashed lines: IoT device to local PDC links, dash-dotted lines: inter-device links, dash-dot-dotted lines: IoT clouds to central PDC links. D.Tx.: Distribution transformer, G.Tx.: Generation transformer.

of corona impulses is assumed to be unit jump counting process. Thus, the pulse arrivals $\Lambda_{\alpha_c} = \{\tau_{\alpha_c,\beta_c} : \beta_c \in \mathbb{N}_{\mathbb{c}}\}$ can be considered to constitute a Poisson time point process [10]. Following similar arguments, it can be concluded without any loss of generality that the impulse source generation in a high voltage outdoor scenario (as in high voltage transmission lines) is also a Poisson time point process with parameter λ_s, which is the rate of generation of impulse sources.

The PMUs are considered optimally placed as suggested in [29], for making the power system both observable and controllable. Thus, the data redundancy is already quite less. Therefore, these devices need to communicate amongst themselves for complete situational awareness and arresting the faults (cf. Fig. 1). Since the data is dynamic and critical, a misinterpretation due to channel errors could be detrimental. In addition to the impairment due to CIN, since the inter PMU communication uses the same channel frequency, it causes CCI which is significant in large-scale IoT deployment [30]. In Fig. 1, the dash-dotted lines show the inter-device communication which is the major source of CCI in our analysis, while the dashed and dash-dot-dotted lines denote the PMU to local PDC and local PDC to central PDC communications, respectively.

In this paper, a Nakagami-m faded wireless link carrying these data is analyzed under four noise profiles: (1) CCI and additive white Gaussian noise (AWGN), (2) CIN and AWGN, (3) CCI, CIN, AWGN, and (4) pure AWGN. All CIS are supposed to have multiple impulse states and traverse a fading channel to the receiver. Similarly, the IoT devices cause CCI at the receiver. We assume cluster for IoT devices that are in vicinity of each other with the size varying between $[1, \overline{N}_I]$, where N_I is the number of devices communicating in the window of duration ΔT. This clustering is purely based on the PMU placements and the path loss factor that the device data transmission would face. Throughout the analysis, we have assumed that these devices are intelligently communicating, and therefore all devices are not active at the same time.

III. Statistical Modeling of CIN and CCI

In this section we study the CIN and CCI statistics. The key notations are listed in Table I.

A. CIN Modeling

In a time window T with reference at $t = 0$, let A_c be the total number of time-varying impulse sources with each source contributing B_{α_c} impulse states. Also, let d_{α_c} be the distance of the α_c-th impulse noise source from the receiver with path loss exponent $\eta \in [2, 4]$. If h_{α_c,β_c}

TABLE I: List of notations used with their descriptions

A_c	Total number of time varying CIN sources
B_{α_c}	Total number of impulse states for the α_c-th source, $\alpha_c \in [1, A_c]$, $\beta_c \in [1, B_{\alpha_c}]$
d_{α_c}	Distance of α_c-th CIN source from receiver
η	Power path loss exponent, $\eta \in [2, 4]$
$h_{\alpha_c,\beta_c} e^{\theta_{\alpha_c,\beta_c}}$	Channel impulse response at receiver due to β_c-th impulse from α_c-th source
$F_{\alpha_c,\beta_c} e^{j\phi_{\alpha_c,\beta_c}}$	Receiver narrow-band filtering for power system impulse noise
T_{α_c,β_c}, τ_{α_c,β_c}	Duration of β_c-th impulse from α_c-th source referenced at $t = 0$
$\mathbb{1}(\cdot)$	Indicator ensuring activity of the impulse referenced at τ_{α_C,β_c}
T	Observation time frame for CIN modeling
ω_I, ω_Q	Characteristic function variables for in-phase and quadrature components $\mathscr{C}^I$ and $\mathscr{C}^Q$
(λ_s, μ_s), (λ_I, μ_I)	Rate of generation and mean life couple for CIN sources and impulses per source
p, q	Number of interferer clusters and interferers per cluster
D, Q_p	Random number of active clusters and active interferer/cluster, $p \in [1, D]$, $q \in [1, Q_p]$
$g_{p,q}$, $X_{p,q}$	i.i.d. random fast fading and random emission respectively by interferer q of cluster p
λ, λ_p, μ_p, r_e	Rate of generation of CCI sources and impulses/source, mean life of impulse, cluster radius
P_t, P_r, P_I, P_n	Power of transmitted signal, received signal, impulse noise, and receiver thermal noise

is the channel impulse response for the α_c-th source-receiver pair as seen by the β_c-th impulse rendered by the α_c-th source, total EMN contribution at the receiver using the echo model is

$$\mathscr{C}(T) = \sum_{\alpha_c=1}^{A_c} d_{\alpha_c}^{-\eta/2} \sum_{\beta_c=1}^{B_{\alpha_c}} h_{\alpha_c,\beta_c} e^{j\theta_{\alpha_c,\beta_c}} X_{\alpha_c,\beta_c} \tag{2}$$

where $X_{\alpha_c,\beta_c} = F_{\alpha_c,\beta_c} e^{j\phi_{\alpha_c,\beta_c}} \mathbb{1}(\tau_{\alpha_c,\beta_c} \leq T^c_{\alpha_c,\beta_c})$ is the impulse duration dependent β_c-th impulse emission with $F_{\alpha_c,\beta_c} e^{j\phi}$ the narrow-band filtering at the receiver, and $\mathbb{1}(\cdot)$ is the indicator function ensuring the activity of the impulse referenced at τ_{α_c,β_c}. Substituting this value in (2) we obtain

$$\mathscr{C}(T) = \sum_{\alpha_c=1}^{A_c} \sum_{\beta_c=1}^{B_{\alpha_c}} d_{\alpha_c}^{-\eta/2} h_{\alpha_c,\beta_c} F_{\alpha_c,\beta_c} \mathbb{1}(\tau_{\alpha_c,\beta_c} \leq T^{\mathbb{C}}_{\alpha_c,\beta_c}) \Big[\cos(\theta_{\alpha_c,\beta_c} + \phi_{\alpha_c,\beta_c}) + j \sin(\theta_{\alpha_c,\beta_c} + \phi_{\alpha_c,\beta_c}) \Big].$$

This is a complex quantity carrying the in-phase ($\mathscr{C}^I$) and quadrature components ($\mathscr{C}^Q$) of the total noise at the receiver. $\mathscr{C}^Q$ is the factor contributing to the propagation of noise, whereas $\mathscr{C}^I$ is the energy impact term. The characteristic function of $\mathscr{C}$ is formulated as

$$\begin{aligned} \Phi_{\mathscr{C}}(\omega) = \mathbb{E}_\varphi \left\{ e^{j\omega_I \mathscr{C}^I} . e^{j\omega_Q \mathscr{C}^Q} \right\} = \mathbb{E}_\varphi \Bigg\{ \exp \Bigg[j \sum_{\alpha_c=1}^{A_c} \sum_{\beta_c=1}^{B_{\alpha_c}} d_{\alpha_c}^{-\eta/2} h_{\alpha_c,\beta_c} F_{\alpha_c,\beta_c} \mathbb{1}(\tau_{\alpha_c,\beta_c} \leq T^{\mathbb{C}}_{\alpha_c,\beta_c}) \\ \times |\omega| \cos(\theta_{\alpha_c,\beta_c} + \phi_{\alpha_c,\beta_c} + \omega_\phi) \Bigg] \Bigg\}. \end{aligned} \tag{3}$$

$|\omega| = \sqrt{{\omega_I}^2 + {\omega_Q}^2}$, $\omega_\phi = \arctan(\omega_Q / \omega_I)$. The expectation is taken over the set $\varphi = \{A_c, B_{\alpha_c}, h_{\alpha_c,\beta_c}, F_{\alpha_c,\beta_c}, \tau_{\alpha_c,\beta_c}, T^{\mathbb{E}}_{\alpha_c,\beta_c}, \theta_{\alpha_c,\beta_c}, \phi_{\alpha_c,\beta_c}\}$. We now bifurcate the CIN modeling under two cases.

1) Independent and Identically Distributed (i.i.d.) CIN Sources: This is a good model when the corona noise sources are distributed along a ring main or parallel feeder power system, in which case the impulse sources behave identically with respect to the receiver noise. By our earlier premise we can infer that the CIS are Poisson distributed as $\alpha \sim Pois(\lambda_s T)$ with an average CIS life μ_s. Taking an expectation over the number of CIS in (3), it can be expressed as

$$\Phi_{\mathscr{C}}(\omega) = \sum_{A_c=0}^{\infty} \frac{e^{-\lambda_s T}(\lambda_s T)^{A_c}}{A_c!} \left(\mathbb{E}\Big\{ \exp\Big[j \sum_{\beta_c=1}^{B} d^{-\eta/2} h_{\beta_c} F_{\beta_c} \mathbb{1}(\tau_{\beta_c} \leq T_{\beta_c}^{\mathbb{C}}) |\omega| \cos(\theta_{\beta_c} + \phi_{\beta_c} + \omega_\phi) \Big] \Big\} \right)^{A_c}.$$

Also, since the sources are identical, the expectation reduces to

$$\Phi_{\mathscr{C}}(\omega) = e^{\lambda_s T \left[\left(\mathbb{E}\Big\{ \exp\Big[j \sum_{\beta_c=1}^{B} d^{-\eta/2} h_{\beta_c} F_{\beta_c} \mathbb{1}(\tau_{\beta_c} \leq T_{\beta_c}^{\mathbb{C}}) \times |\omega| \Big[\cos(\theta_{\beta_c} + \phi_{\beta_c} + \omega_\phi) \Big] \Big\} \right) - 1 \right]}. \tag{4}$$

Generating the log characteristic function $\Psi_{\mathscr{C}}(\omega) = \frac{1}{\lambda_s T} \log \Phi_{\mathscr{C}}(\omega) + 1$ from (4), and taking expectation on the number of impulses per source, with λ_I and μ_I defined as the rate of generation of impulses from CISs and their average life time respectively, we have

$$\begin{aligned} \Psi_{\mathscr{C}}(\omega) &= \mathbb{E}\Big\{ \exp\Big[j \sum_{\beta_c=1}^{B} d^{-\eta/2} h_{\beta_c} F_{\beta_c} \mathbb{1}(\tau_{\beta_c} \leq T_{\beta_c}^{\mathbb{C}}) \times |\omega| \Big[cos(\theta_{\beta_c} + \phi_{\beta_c} + \omega_\phi) \Big] \Big] \Big\} \\ &= \sum_{B=0}^{\infty} \frac{e^{-\lambda_I T}(\lambda_I T)^B}{B!} \left(\mathbb{E}\Big\{ \exp\Big[j d^{-\eta/2} h F \mathbb{1}(\tau \leq T^{\mathbb{C}}) \times |\omega| \Big[\cos(\theta + \phi + \omega_\phi) \Big] \Big\} \right)^B. \end{aligned} \tag{5}$$

The subscripts α_c and β_c are dropped from (5) as all CISs are identical and render the same number of impulses (i.e., $B_{\alpha_c} = B$) owing to the i.i.d. assumption. Using the first order exponential approximation for the Bessel function of zeroth order and first kind, and taking the expectation on the Poisson distributed ($\sim$ Pois($\lambda_I T$)) impulses per source, we get

$$\begin{aligned} \Psi_{\mathscr{C}}(\omega) &= e^{\lambda_I T \left[\left(\mathbb{E}\{ \exp[j d^{-\eta/2} h F \mathbb{1}(\tau \leq T^{\mathbb{C}}) \times |\omega| [\cos(\theta + \phi + \omega_\phi)] | B \} \right) - 1 \right]} \overset{(a)}{=} e^{\lambda_I \mu_I [-1 + e^{-|\omega|^2 d^{-\eta} \mathbb{E}\{h^2 F^2\}}]} \\ &\overset{(b)}{=} e^{-\lambda_I \mu_I} \cdot e^{\lambda_I \mu_I . e^{\frac{-|\omega|^2 \Omega_c d^{-\eta}}{4}}}. \end{aligned} \tag{6}$$

Here, (a) follows from the expectation over the impulse duration τ, reference window T, and the arguments of the cosine function. (b) follows by taking expectation of h^2F^2, where hF is Nakagami-m distributed such that $hF \sim$ Nakagami(m, Ω_c) with $k = m$ and $\theta = \frac{\Omega_c}{m}$. Since, h^2F^2 follows a gamma distribution with parameter. Substituting this reduced form of the exponent in

(4) and rearranging the terms including A_c and B under the double summation, we get a known form in (7).

$$\Phi_{\mathscr{C}}(\omega)=\sum_{A_c=0}^{\infty}\frac{e^{-\lambda_s T}(\lambda_I\mu_I)^{A_c}}{A_c!}\sum_{B=0}^{\infty}\frac{B^{A_c}.(\lambda_s T)^B}{B!}e^{-B.\lambda_I\mu_I}e^{\frac{-A_c|\omega|^2 d^{-\eta}\Omega_c}{4}}=\sum_{A_c=0}^{\infty}\mathbb{P}_{A_c,iso}e^{-\frac{|\omega|^2\sigma^2_{A_c,iso}}{2}} \tag{7}$$

which is the characteristic function of an isotropic Gaussian mixture model. De-energizing (7) using Parseval's theorem we have the density function: $f_{\mathscr{C}}(x)=\sum_{A_c=0}^{A_{\max}}\frac{\mathbb{P}_{A_c,iso}}{\sqrt{2\pi\sigma^2_{A_c,iso}}}e^{-\frac{x^2}{2\sigma^2_{A_c,iso}}}$. It can be generalized to $g_{\mathscr{C}}(x)=\sum_{A_c=0}^{A_{\max}}\frac{\mathbb{W}_{A_c,iso}}{\sqrt{2\pi\sigma^2_{A_c,iso}}}e^{-\frac{x^2}{2\sigma^2_{A_c,iso}}}$, where $\mathbb{W}_{A_c,iso}=\frac{\mathbb{P}_{A_c,iso}}{\sum_{A_c=1}^{A_{\max}}\mathbb{P}_{A_c,iso}}$ is the weight of each mixture component. $\mathbb{P}_{A_c,iso}=\frac{e^{-\lambda_s T}(\lambda_I\mu_I)^{A_c}}{A_c!}\sum_{B=0}^{\infty}\frac{B^{A_c}(\lambda_s T)^B}{B!}e^{-B\lambda_I\mu_I}$ is the weight of the Gaussian mixture model with infinite components, and $\sigma^2_{A_c,iso}=A_c.\mathbb{E}_{h,F}\{d^{-\eta}h^2F^2\}/2$ is the power of each component. Below, we address the CIN modeling in the second case.

2) Independent but Non-Identically Distributed CIN Sources: This model is suited for power transmission scenarios where the CISs could be sporadically located. Under similar premise as before, we take the expectation on randomness of the number of CISs which yields

$$\begin{aligned}\Phi_{\mathscr{C}}(\omega)=\sum_{A_c=0}^{\infty}\frac{e^{-\lambda_s T}(\lambda_s T)^{A_c}}{A_c!}\prod_{\alpha_c=1}^{A_c}\mathbb{E}\Bigg\{\exp\Bigg[j\sum_{\beta_c=1}^{B_{\alpha_c}}d_{\alpha_c}^{-\eta/2}h_{\alpha_c,\beta_c}F_{\alpha_c,\beta_c}\mathbb{1}(\tau_{\alpha_c,\beta_c}\leq T^{\mathbb{C}}_{\alpha_c,\beta_c})|\omega|\\ \times\Big[\cos(\theta_{\alpha_c,\beta_c}+\phi_{\alpha_c,\beta_c}+\omega_\phi)\Big]\Bigg]\Bigg\}.\end{aligned} \tag{8}$$

Evaluating the expectation in (8) over the number of impulses β_c from the α_c-th source, we have

$$\begin{aligned}\Psi_{\mathscr{C}}(\omega)&=\mathbb{E}\left\{\exp\left[j\sum_{\beta_c=1}^{B_{\alpha_c}}d_{\alpha_c}^{-\eta/2}h_{\alpha_c,\beta_c}F_{\alpha_c,\beta_c}\mathbb{1}(\tau_{\alpha_c,\beta_c}\leq T^{\mathbb{C}}_{\alpha_c,\beta_c})|\omega|\cos(\theta_{\alpha_c,\beta_c}+\phi_{\alpha_c,\beta_c}+\omega_\phi)\right]\right\}\\ &\overset{(c)}{=}\exp\left(-\lambda_{\alpha_c}\mu_{\alpha_c}\right)\sum_{B_{\alpha_c}=0}^{\infty}\frac{(\lambda_{\alpha_c}\mu_{\alpha_c})^{B_{\alpha_c}}}{B_{\alpha_c}!}\times\exp\left(-|\omega|^2\left\{\frac{B_{\alpha_c}\mathbb{E}[d_{\alpha_c}^{-\eta}h^2_{\alpha_c,\beta_c}F^2_{\alpha_c,\beta_c}]}{4}\right\}\right)\end{aligned} \tag{9}$$

where λ_{α_c} and μ_{α_c} are respectively the rate of generation of impulses and their average life time for the α_c-th source. (c) in (9) follows from taking the expectation over τ_{α_c,β_c}, and the arguments of the cosine function. A close scrutiny of (9) reveals that this is the characteristic function of a single corona noise producing source with infinite impulse count in the frame of interest, which is a Gaussian mixture model. Substituting the expression in (8) and rearranging, we have

$$\Phi_{\mathscr{C}}(\omega)=\sum_{A_c=0}^{\infty}\frac{e^{-\lambda_s T}(\lambda_s T)^{A_c}}{A_c!}\prod_{\alpha_c=1}^{A_c}e^{-\lambda_{\alpha_c}\mu_{\alpha_c}}\sum_{B_{\alpha_c}=0}^{\infty}\frac{(\lambda_{\alpha_c}\mu_{\alpha_c})^{B_{\alpha_c}}}{B_{\alpha_c}!}e^{-B_{\alpha_c}|\omega|^2\frac{\mathbb{E}\{d_{\alpha_c}^{-\eta}\boldsymbol{h}^2_{\alpha_c,\beta_c}F^2_{\alpha_c,\beta_c}\}}{4}}. \tag{10}$$

Let, $\prod_{\alpha_c=1}^{A_c}\left(\sum_{B_{\alpha_c}=0}^{\infty}\frac{(\lambda_{\alpha_c}\mu_{\alpha_c})^{B_{\alpha_c}}}{B_{\alpha_c}!}e^{-B_{\alpha_c}|\omega|^2\frac{\mathbb{E}\{d_{\alpha_c}^{-\eta}h_{\alpha_c}^2F_{\alpha_c}^2\}}{4}}\right)\overset{(def)}{=}\zeta(\omega)$, $\lambda_{\alpha_c}\mu_{\alpha_c}\overset{(def)}{=}R_{\alpha_c}$, $\mathbb{E}\{d_{\alpha_c}^{-\eta}h_{\alpha_c}^2F_{\alpha_c}^2\}\overset{(def)}{=}S_{\alpha_c}$, and $R_{\alpha_c}e^{-|\omega|^2S_{\alpha_c}}\overset{(def)}{=}C_{\alpha_c}$. Then, $\zeta(\omega)=(\sum_{B_1=0}^{\infty}\frac{C_1{}^{B_1}}{B_1!})\times\cdots\times(\sum_{B_A=0}^{\infty}\frac{C_A{}^{B_A}}{B_A!})=e^{\sum_{\alpha=1}^{A}C_{\alpha_c}}$, using term-wise Taylor contraction. For smaller channel noise power, $C_{\alpha_c}\approx R_{\alpha_c}(1-|\omega|^2S_{\alpha_c})$ and hence $\zeta(\omega)\approx e^{\sum_{\alpha_c=1}^{A_c}R_{\alpha_c}}.e^{-\sum_{\alpha_c=1}^{A_c}|\omega|^2R_{\alpha_c}S_{\alpha_c}}$. Thus (10) simplifies to

$$\begin{aligned}\Phi_{\mathscr{C}}(\omega)&=\sum_{A_c=0}^{\infty}e^{-(\lambda_sT+\sum_{\alpha_c=1}^{A_c}\lambda_{\alpha_c}\mu_{\alpha_c})}\frac{(\lambda_sT)^{A_c}}{A_c!}e^{\sum_{\alpha_c=1}^{A_c}R_{\alpha_c}}.e^{-\sum_{\alpha_c=1}^{A_c}|\omega|^2R_{\alpha_c}S_{\alpha_c}}\\&=\sum_{A_c=0}^{\infty}e^{-\lambda_sT}\frac{(\lambda_ST)^{A_c}}{A_c!}.e^{-|\omega|^2\sum_{\alpha_c=1}^{A_c}\frac{\lambda_{\alpha_c}\mu_{\alpha_c}}{4}\mathbb{E}\{d_{\alpha_c}^{-\eta}h_{\alpha_c}^2F_{\alpha_c}^2\}}=\sum_{A_c=0}^{\infty}\mathbb{P}_{A_c,mca}e^{-\frac{|\omega|^2\sigma_{A_c,mca}^2}{2}}.\end{aligned}\tag{11}$$

(11) represents the Middleton class-A model's [31] characteristic function. By Parseval's identity it yields $f_{\mathscr{C}}(x)=\sum_{A_c=0}^{A_{\max}}\frac{\mathbb{P}_{A_c,mca}}{\sqrt{2\pi\sigma_{A_c,mca}^2}}e^{-\frac{x^2}{2\sigma_{A_c,mca}^2}}$. It can be generalized under practical constraints as $g_{\mathscr{C}}(x)=\sum_{A_c=0}^{A_{\max}}\frac{\mathbb{W}_{A_c,mca}}{\sqrt{2\pi\sigma_{A_c,mca}^2}}e^{-\frac{x^2}{2\sigma_{A_c,mca}^2}}$, where $\mathbb{W}_{A_c,mca}=\frac{\mathbb{P}_{A_c,mca}}{\sum_{A_c=1}^{A_{\max}}\mathbb{P}_{A_c,mca}}$ is the contribution of each mixture component, with $\mathbb{P}_{A_c,mca}=\frac{e^{-\lambda_sT}(\lambda_sT)^{A_c}}{A_c!}$ and $\sigma_{A_c,mca}^2=\sum_{\alpha_c=1}^{A_c}\frac{\lambda_{\alpha_c}\mu_{\alpha_c}}{2}\mathbb{E}\{d_{\alpha_c}^{-\eta}h_{\alpha_c}^2F_{\alpha_c}^2\}$.

The above models capture the total corona noise contribution at a wireless receiver under different CIN source statistics, to be discussed in Section VI. Next, we develop the CCI model.

B. CCI Modeling

Consider a scenario where multiple power system IoT devices, viz., PMUs, smart meters, smart circuit breakers are trying to communicate. The interferers are distributed as spatial Poisson point process (PPP) over the interference space $\mathscr{T}$. Let p be the number of interferers clusters which can be differently located in space-time, and q be the number of interferers in each cluster in the time window T. Then, total interference at the receiver may be expressed as,

$$Y(t)=\sum_{p=1}^{D}\sum_{q=1}^{Q_p}d_{p,q}^{-\eta/2}h_{p,q}F_{p,q}e^{j(\theta_{p,q}+\phi_{p,q})}\tag{12}$$

where $g_{p,q}=h_{p,q}e^{j\theta_{p,q}}$ is the i.i.d. random fast fading as seen by interferer q of cluster p, D is the random number of active interferer clusters, $d_{p,q}$ is the random distance of an active interferer, and η is the path loss exponent. $X_{p,q}=F_{p,q}e^{j\phi_{p,q}}$ is the random emission by interferers. Also, $F_{p,q}$ and $\phi_{p,q}$ are respectively the i.i.d. emission envelope and i.i.d. random and uniformly distributed phase of emissions where $\phi_{p,q}\in[0,2\pi]$. The joint characteristic function for the total interference

at the receiver due to all these sources, similarly as formulated in Subsection III-A, is given as

$$\Phi_Y(\omega) = \mathbb{E}_{\varphi}\Big\{ \exp\Big[j|\omega| \sum_{p=1}^{D} \sum_{q=1}^{Q_p} d_{p,q}^{-\eta/2} h_{p,q} F_{p,q} \times \Big[\cos(\theta_{p,q} + \phi_{p,q} + \omega_{\phi}) \Big] \Big\} \tag{13}$$

where the expectation is over the set $\varphi = \{p, q, h_{p,q}, F_{p,q}, \theta_{p,q}, \phi_{p,q}\}$. Since the CCI sources are PPP distributed with intensity λ, the expectation over p can be expressed as

$$\begin{aligned} \Phi_Y(\omega) &= \sum_{D=0}^{\infty} \mathbb{E}_{\varphi}\Big\{ \exp\Big[j|\omega| \sum_{p=1}^{D} \sum_{q=1}^{Q_p} d_{p,q}^{-\eta/2} h_{p,q} F_{p,q} \cos(\theta_{p,q} + \phi_{p,q} + \omega_{\phi}) \Big\} \frac{(\lambda \pi r_e^2)^D e^{-\lambda \pi r_e^2}}{D!} \\ &\overset{(d)}{=} \sum_{D=0}^{\infty} \prod_{p=1}^{D} \Psi_Y(\omega) (\lambda \pi r_e^2)^D \frac{e^{-\lambda \pi r_e^2}}{D!}. \end{aligned} \tag{14}$$

Here r_e is the effective radius of the IoT device cluster area, and $\Psi_Y(\omega) \overset{(def)}{=} \mathbb{E}\Big\{ \exp\Big[j|\omega| \times \sum_{q=1}^{Q_p} d_{p,q}^{-\eta/2} h_{p,q} F_{p,q} \times \cos(\theta_{p,q} + \phi_{p,q} + \omega_{\phi}) \Big] \Big\}$ is the characteristic function for interference per cluster. Note that, since the CCI sources are independent, the product over p can be taken out of the expectation, resulting in (d). With the expectation over p taken in (14), p is dropped from the expectation set, thus $\varphi = \{q, h_{p,q}, F_{p,q}, \theta_{p,q}, \phi_{p,q}\}$. Taking the expectation over q we have

$$\begin{aligned} \Psi_Y(\omega) =& \mathbb{E}\Big\{ \exp\Big[j|\omega| \sum_{q=1}^{Q_p} d_{p,q}^{-\eta/2} h_{p,q} F_{p,q} \cos(\theta_{p,q} + \phi_{p,q} + \omega_{\phi}) \Big] \Big\} \\ &\overset{(e)}{=} \sum_{Q_p=0}^{\infty} \prod_{q=1}^{Q_p} \mathbb{E}\Big\{ \exp\Big[j|\omega| d_{p,q}^{-\eta/2} h_{p,q} F_{p,q} \cos(\theta_{p,q} + \phi_{p,q} + \omega_{\phi}) \Big] \Big\} e^{-G_p} \frac{G_p^{Q_p}}{Q_p!} \\ &\overset{(f)}{=} \sum_{Q_p=0}^{\infty} \Big(\mathbb{E}\Big\{ \exp\Big[j|\omega| d_p^{-\eta/2} h_p F_p \cos(\theta_p + \phi_p + \omega_{\phi}) \Big] \Big\} \Big)^{Q_p} e^{-G_p} \frac{G_p^{Q_p}}{Q_p!}. \end{aligned} \tag{15}$$

(e) results from taking expectation over the number of active interferers q in cluster p, with $G_p = \lambda_p \mu_p$ and $\mu_p = \mathbb{E}[T]$. The expectation set now reduces to $\varphi = \{h_{p,q}, F_{p,q}, \theta_{p,q}, \phi_{p,q}\}$. Since the emissions are considered i.i.d., we can take out the summation operator in the exponent in the form of a product outside the expectation, as in (e). Further, under the premise of independence

the product is replaced by power Q_p, as in (f). By rearranging (15)(f) we have

$$\begin{aligned}\Psi_Y(\omega) =& e^{-G_p}\sum_{Q_p=0}^{\infty}\frac{\left(G_p\mathbb{E}\left\{\exp\left[j|\omega|d_p^{-\eta/2}h_pF_p\cos(\theta_p+\phi_p+\omega_\phi)\right]\right\}\right)^{Q_p}}{Q_p!}\\ \overset{(g)}{=}& \exp\left\{G_p\left[\mathbb{E}\left\{\exp\left[j|\omega|d_p^{-\eta/2}h_pF_p\cos(\theta_p+\phi_p+\omega_\phi)\right]\right\}-1\right]\right\}\\ \overset{(h)}{=}& \exp\left\{G_p\left(\zeta_Y(\omega)-1\right)\right\}.\end{aligned} \tag{16}$$

(g) uses the Taylor series expansion result. $\zeta_Y(\omega)\overset{(def)}{=}\mathbb{E}\left\{\exp\left[j|\omega|d_p^{-\eta/2}h_pF_p\cos(\theta_p+\phi_p+\omega_\phi)\right]\right\}$. Using Jacobi-Anger identity, we have: $\exp\{ja\cos(\theta)\}=\sum_{i=0}^{\infty}j^i\epsilon_iJ_i(a)\cos(i\theta)$, where a is an arbitrary constant and J_i is the Bessel's function of i-th order, with $\epsilon_0=1$ and $\epsilon_k=2\ \forall k\geq 1$,

$$\begin{aligned}\zeta_Y(\omega) =& \mathbb{E}\left\{\exp\left[j|\omega|d_p^{-\eta/2}h_pF_p\cos(\theta_p+\phi_p+\omega_\phi)\right]\right\}\\ \overset{(k)}{=}& \mathbb{E}\left\{\sum_{i=0}^{\infty}j^i\epsilon_iJ_i(|\omega|d_p^{-\eta/2}h_pF_p)\cos(i(\theta_p+\phi_p+\omega_\phi))\right\}.\end{aligned} \tag{17}$$

(17)(k) results from Jacobi-Anger expansion. Also, it is notable that the expectation of cosine function over $\{\theta,\phi\}\in\varphi$ is zero $\forall i\geq 1$ because of its symmetry. Hence, (17) reduces to

$$\zeta_Y(\omega)=\mathbb{E}\left\{J_0(|\omega|d_p^{-\eta/2}h_pF_p)\right\}\overset{(l)}{\approx}e^{-\frac{|\omega|^2\mathbb{E}[d_p^{-\eta}h_p^2F_p^2]}{4}}. \tag{18}$$

(18)(l) follows from the approximation for expectation over the Bessel's function of zeroth order, and the expectation set reduces to $\varphi=\{h_p,F_p\}$. Therefore, substituting (18) in (16) we have

$$\Psi_Y(\omega)=\exp\left\{G_p\left(e^{-\frac{|\omega|^2\mathbb{E}_\varphi[d_p^{-\eta}h_p^2F_p^2]}{4}}-1\right)\right\}=\exp\left\{\lambda_p\mu_p\left(e^{-\frac{|\omega|^2\mathbb{E}[d_p^{-\eta}h_p^2F_p^2]}{4}}-1\right)\right\}. \tag{19}$$

Substituting (19) in (14) we have

$$\begin{aligned}\Phi_Y(\omega) =& \sum_{D=0}^{\infty}\prod_{p=1}^{D}e^{\lambda_p\mu_p\left\{e^{\frac{|\omega|^2\mathbb{E}[d_p^{-\eta}h_p^2F_p^2]}{4}}-1\right\}}\frac{S^De^{-S}}{D!}\\ \overset{(m)}{\approx}& \sum_{D=0}^{\infty}\prod_{p=1}^{D}e^{\lambda_p\mu_p\left\{1-\frac{|\omega|^2\mathbb{E}[d_p^{-\eta}h_p^2F_p^2]}{4}+\mathcal{O}(|\omega|^4)-1\right\}}\frac{S^De^{-S}}{D!}\\ \overset{(n)}{=}& \sum_{D=0}^{\infty}\frac{S^De^{-S}}{D!}e^{\left\{-|\omega|^2\sum_{p=1}^{D}\lambda_p\mu_p\mathbb{E}[d_p^{-\eta}h_p^2F_p^2]/4\right\}}=\sum_{D=0}^{\infty}\mathbb{P}_{\mathbb{D}}e^{-\frac{|\omega|^2\sigma_D^2}{2}}\end{aligned} \tag{20}$$

where $S=\lambda\pi r_e^2$ denotes the cluster area. (20)(m) follows from the Taylor series approximation of the exponential having $|\omega|^2$ in the power. (20)(n) results from rearranging the terms in (20)(m)

such that $\mathbb{P}_D = \frac{S^D e^{-S}}{D!}$, a Poisson distributed weight. $\sigma_D^2 = \sum_{p=1}^{D} \lambda_p \mu_p \mathbb{E}[d_p^{-\eta} h_p^2 F_p^2]/2$ is the variance of the density function or alternatively the power of the D-th CCI interferer. This is the characteristic function for Middleton class-A model which yields the density function using Parseval's theorem. Generalizing to finite terms, the density is found as $g_Y(x) = \sum_{D=1}^{D_{\max}} \frac{\mathbb{W}_D}{\sqrt{2\pi\sigma_D^2}} e^{-\frac{x^2}{2\sigma_D^2}}$, with $\mathbb{W}_D = \frac{\mathbb{P}_D}{\sum_{D=1}^{D_{\max}} \mathbb{P}_D}$ being the weights of the mixture components in the finitely truncated Middleton class-A model. Modeling of CCI is done by invoking the system model assumptions in Section II. We have now formulated the statistical models for the noises constituting the 4 cases. Section IV will use the expressions (11) and (20) respectively for CIN and CCI analyses.

IV. Outage Probability Analysis

In communication channel, due to fading or variable channel characteristic over space-time, sometimes the information rate may fall below a given threshold, leading to signal outage. We now derive the outage probability along with the intermediate parameters' distributions.

A. Total Unwanted Power Distribution

An exact expression of total unwanted power over communication channel in smart grid environment is derived considering different noises. Exact expression is important for understanding the different noise profiles and analyzing the performance parameters subsequently.

Lemma 1. *The sum of two random variables following gamma mixture model and gamma distribution respectively is a random variable with a raised dimension gamma mixture model.*

Proof. Let x be modeled as a gamma mixture and y be a gamma distributed random variable, as would be the scenario in the distribution of total unwanted power in a highly impulsive noise or interference limited environment. The associated moment generating function is expressed as,

$$M(t) = \sum_{i=1}^{N} \omega_i (1 - \beta_i^{\mathbb{1}} t)^{-\alpha_i^{\mathbb{1}}} \times (1 - \beta_2 t)^{-\alpha_2}. \tag{21}$$

$(\alpha_i^{\mathbb{1}}, \beta_i^{\mathbb{1}})$ and (α_2, β_2) are the shape and rate parameter couples respectively for the gamma mixture model and gamma distribution. Using the approach in [32] and inverting (21) term by term, the distribution of $z = x + y$ is derived as,

$$f(z) = \sum_{i=1}^{N} \omega_i \Big(\frac{\beta_{1,i}}{\beta_{2,i}}\Big)^{1/2} \sum_{k=0}^{\infty} \frac{\delta_k}{k! \beta_{1,i}^{k+1}} x^k e^{-x/\beta_{1,i}} \tag{22}$$

where $\beta_{1,i} = \min(\beta_i^{\mathbb{1}}, \beta_2)$ and $\beta_{2,i} = \beta_{1,i}^{'}$ is the complement of $\beta_{1,i}$. □

Remark 1. *It must be noted here that though the summation running over k in Lemma 1 and all other subsequent analysis that follow from Lemma 1 have infinite summation lengths, in practice these summations converge over a finite boundary, which has been analytically proven in [32]. Under the premise of uniform convergence proved for the summation over k in the case of the distribution for the sum of gamma distributed random variables in [32], we can call this exact expression and the subsequent results closed-form for all practical implementation purposes, as the number of summands becomes finite, with a definite analytical guarantee on their convergence.*

Using Lemma 1, the distribution of total unwanted power z can be expressed as

$$\text{CCI+AWGN: } f_Z(z) = \sum_{D=1}^{D_{\max}} \mathbb{W}_D \Big(\frac{\beta_{1,D}}{\beta_{2,D}}\Big)^{1/2} \sum_{k=0}^{\infty} \frac{\delta_k}{k! {\beta_{1,D}}^{k+1}} z^k . e^{-z/\beta_{1,D}}$$

$$\text{CIN+AWGN: } f_Z(z) = \sum_{A_c=0}^{A_{\max}} \mathbb{W}_{A_c,mca} \Big(\frac{\beta_{1,A_c}}{\beta_{2,A_c}}\Big)^{1/2} \sum_{k=0}^{\infty} \frac{\delta_k}{k! {\beta_{1,A_c}}^{k+1}} z^k . e^{-z/\beta_{1,A_c}}$$

$$\text{CCI+CIN+AWGN: } f_Z(z) = \sum_{A_c=0}^{A_{\max}} \mathbb{W}_{A_c,mca} \sum_{D=1}^{D_{\max}} \mathbb{W}_D \sum_{k_1=0}^{\infty} \delta_{k_1} \Big(\frac{\beta_{1,D,A_c}}{\beta_{2,D,A_c}}\Big)^{1/2} \sum_{k_2=0}^{\infty} \Big(\frac{\beta_{\min}}{\beta_{\max}}\Big)^{k_1+1} \times \frac{\delta_{k_2} z^{k_1+k_2+1/2}}{\Gamma(k_1+k_2+3/2)(\beta_{\min})^{k_1+k_2+3/2}} . e^{-z/\beta_{\min}}$$

where σ^2_{AWGN} is the AWGN channel variance and $\delta_{k+1} = \frac{1}{k+1} \sum_{i=1}^{k+1} i \mathscr{H}_i \delta_{k+i-1}$, with $\delta_0 = 1$, $\mathscr{H}_i = \sum_{j=1}^{2} \alpha_j (1 - \beta_{1,i}/\beta_j)^i / i$, $\beta_{1,D} = \min\{\sigma^2_D, \sigma^2_{AWGN}\}$, $\beta_{1,A_c} = \min\{\sigma^2_{A_c,mca}, \sigma^2_{AWGN}\}$, $\beta_{\min} = \min\{\beta_{1,D,A_c}, 2\sigma^2_{AWGN}\}$, $\beta_{\max} = \max\{\beta_{1,D,A_c}, 2\sigma^2_{AWGN}\}$, and $\beta_{1,D,A_c} = \min\{\sigma^2_D\ , \sigma^2_{A_c,mca}\}$.

B. Signal-to-Pulse-Noise Ratio (SPNR) Distribution

SPNR is defined as the ratio of signal to unwanted power in an impulsive noise environment. Mathematically, $\gamma_r^p = \lim_{\Delta t \to 0} P_r / \{P_{I^{\Delta t}} + P_n\}$, where Δt is the pulse width. This is an important parameter in the analysis of wireless communication in presence of power system EMN, which is an indicator of channel capacity in an impulsive noise limited environment. This section aims at deriving an exact form SPNR expression for various noise and interference impaired situations.

Lemma 2. *The ratio of a gamma distributed random variable and a gamma mixture modeled random variable is a random variable with a beta prime mixture model.*

Proof. See Appendix A. □

Using Lemma 2, the SNR or SINR or SPNR distribution $f_\Gamma(\gamma)$ under different smart grid noise profiles for a Nakagami-m faded channel are derived as follows,

$$\text{AWGN:} f_\Gamma(\gamma) = \beta^{'}(\gamma; m, 1/2, 1, P_t\Omega_{channel}/2m\sigma^2_{AWGN})/\sigma^2_{AWGN}$$

$$\text{CCI+AWGN:} f_\Gamma(\gamma) = \sum_{D=1}^{D_{\max}} \mathbb{W}_D\Big(\frac{\beta_{1,D}}{\beta_{2,D}}\Big)^{1/2} \sum_{k=0}^{\infty} \delta_k \beta^{'}\left(\gamma; m, k+1, 1, \frac{P_t\Omega_{channel}}{m\beta_{1,D}}\right)$$

$$\text{CIN+AWGN:} f_\Gamma(\gamma) = \sum_{A_c=0}^{A_{\max}} \mathbb{W}_{A_c,mca}\Big(\frac{\beta_{1,A_c}}{\beta_{2,A_c}}\Big)^{1/2} \sum_{k=0}^{\infty} \delta_k \beta^{'}\left(\gamma; m, k+1, 1, \frac{P_t\Omega_{channel}}{m\beta_{1,A_c}}\right)$$

$$\begin{aligned}\text{CCI+CIN+AWGN:} f_\Gamma(\gamma) = &\sum_{A_c=0}^{A_{\max}} \mathbb{W}_{A_c,mca} \sum_{D=1}^{D_{\max}} \mathbb{W}_D \sum_{k_1=0}^{\infty} \delta_{k_1}\Big(\frac{\beta_{1,D,A_c}}{\beta_{2,D,A_c}}\Big)^{1/2} \sum_{k_2=0}^{\infty} \delta_{k_2}\Big(\frac{\beta_{min}}{\beta_{\max}}\Big)^{k_1+1} \\ &\times \beta^{'}\left(\gamma; m, k_1+k_2+3/2, 1, \frac{P_t\Omega_{channel}}{m\beta_{min}}\right)\end{aligned}$$

where P_t is the transmitted signal power, $\Omega_{channel}$ is the message signal variance, and $\beta^{'}(\gamma;)$ denotes the beta prime distribution of γ.

Remark 2. *Let the variance-mean couple for wanted or message power distribution be (σ^2_W, μ_W) and for the unwanted power be $(\sigma^2_{UW}, \mu_{UW})$. Then, the relative dispersion index (RDI) ξ is defined as $\frac{\sigma^2_W/\mu_W}{\sigma^2_{UW}/\mu_{UW}}$. If the probability distribution has k mixture components with mixing probability π_i for the i-th mixture component, then the CuRD index (q_d) is defined as $q_d = \sum_{i=1}^{k} \pi_i \xi_i$.*

Therefore, the outage probabilities defined as $Pr\{\gamma < \gamma_{th}\} = \int_0^{\gamma_{th}} f_\Gamma(\gamma) d\gamma$ are derived as,

$$\text{AWGN: } Pr\{\gamma < \gamma_{th}\} = \Big(\frac{\gamma_{th}}{q_d P_t}\Big)^m {}_2F_1\Big(m, m+1/2; m+1; -\frac{\gamma_{th}}{q_d P_t}\Big)/mB(m, 1/2)$$

$$\text{CCI+AWGN: } Pr\{\gamma < \gamma_{th}\} = \sum_{D=1}^{D_{\max}} \mathbb{W}_D\Big(\frac{\beta_{1,D}}{\beta_{2,D}}\Big)^{\frac{1}{2}} \sum_{k=0}^{\infty} \delta_k \frac{\Big(\frac{\gamma_{th}}{q_d P_t}\Big)^m {}_2F_1\Big(m, m+k+1; m+1; -\frac{\gamma_{th}}{q_d P_t}\Big)}{mB(m, k+1)}$$

$$\text{CIN+AWGN: } Pr\{\gamma < \gamma_{th}\} = \sum_{A_c=0}^{A_{\max}} \mathbb{W}_{A_c,mca}\Big(\frac{\beta_{1,A_c}}{\beta_{2,A_c}}\Big)^{\frac{1}{2}} \sum_{k=0}^{\infty} \delta_k \frac{\Big(\frac{\gamma_{th}}{q_d P_t}\Big)^m {}_2F_1\Big(m, m+k+1; m+1; -\frac{\gamma_{th}}{q_d P_t}\Big)}{mB(m, k+1)}$$

$$\begin{aligned}\text{CCI+CIN+AWGN: } Pr\{\gamma < \gamma_{th}\} = &\sum_{A_c=0}^{A_{\max}} \mathbb{W}_{A_c,mca} \sum_{D=1}^{D_{\max}} \mathbb{W}_D \sum_{k_1=0}^{\infty} \delta_{k_1}\Big(\frac{\beta_{1,D,A_c}}{\beta_{2,D,A_c}}\Big)^{\frac{1}{2}} \sum_{k_2=0}^{\infty} \delta_{k_2}\Big(\frac{\beta_{min}}{\beta_{\max}}\Big)^{k_1+1} \\ &\times \frac{\Big(\frac{\gamma_{th}}{q_d P_t}\Big)^m {}_2F_1\Big(m, m+k_1+k_2+3/2; m+1; -\frac{\gamma_{th}}{q_d P_t}\Big)}{mB(m, k_1+k_2+3/2)}\end{aligned}$$

where ${}_2F_1(\mathbf{a};\mathbf{b};z)$ is the Gaussian hypergeometric function, γ_{th} is an acceptable SPNR threshold and q_d is the CuRD index for the outage distributions defined as $\frac{\Omega_{channel}}{m\sigma^2_{AWGN}}$, $\frac{\Omega_{channel}}{m\beta_{1,D}}$, $\frac{\Omega_{channel}}{m\beta_{1,A_c}}$, and $\frac{\Omega_{channel}}{m\beta_{min}}$ respectively for AWGN, CCI+AWGN, CIN+AWGN, and CCI+CIN+AWGN profiles.

Remark 3. *Though these distributions look alike, notably the occurrence probabilities of mixture components in their respective probability spaces are different and render different mixture models (see Fig. 3). Also with the increase in number of elements contributing to the unwanted power, the signal space dimension increases, which decides the nature of the distributions.*

Remark 4. *The SPNR distribution manifests to a generalized beta prime distribution which can be intuitively supported from its generation by compounding two gamma distributions (wanted power and unwanted power). Notably, all signal and noise amplitude distributions considered here render a gamma distribution for their respective power profiles. The validity of outage probability stems from the cumulative distribution function of the respective SPNR profiles.*

V. Throughput Analysis

Average throughput is often defined in terms of packet success rate in a radio network. In this section, we analyze the network throughput under various noise and interference profiles by developing a $2L$ state Markov model. The states of the Markov chain are the various SNR or SINR or SPNR thresholds. We use the LCR to find the transition probability from present to future states and AFD as a tool to parameterize the duration of stay in that particular state and generating a count on the number of bits arriving in that channel state. This modeling helps in transiting from physical analysis to the network layer performance characterization.

A. Level Crossing Rate (LCR)

LCR is used to predict the channel state in conjunction with AFD [33], [34]. In this work this will aid in finding the state transition probabilities in the Markov chain in Fig.2.

Lemma 3. *For a Nakagami-m faded channel relaying data in a highly impulsive noise or interference limited environment, the LCR can be modeled as a beta prime mixture distribution, with the mixture components solely dependent on the expected number of noise impulses.*

Proof. See Appendix B. □

B. Average Fade Duration (AFD)

We now derive exact expressions for AFD in different communication scenarios. The AFD expression is used to guide packet length selection to minimize packet error rates.

Using Lemma 3 and the outage probability expressions derived in Section IV, the exact expression of AFD defined as $\bar{t} = \frac{\int_0^R f_\Gamma(\gamma)d\gamma}{LCR}$, where R is the level of interest, is derived as,

$$\text{AWGN: } \bar{t} = \Big(\frac{R}{q_d P_t}\Big)^m \frac{{}_2F_1\Big(m, m+1/2; m+1; -\frac{R}{q_d P_t}\Big)}{mB(m,1/2)} \Big/ \frac{\sigma_{\dot{g}}^2}{\sqrt{2\pi}} \frac{\beta'(R; m, 1/2, 1, \frac{P_t\Omega_{channel}}{2m\sigma^2_{AWGN}})}{\sigma^2_{AWGN}}$$

$$\text{CCI+AWGN: } \bar{t} = \frac{\sum_{D=1}^{D_{\max}} \mathbb{W}_D \Big(\frac{\beta_{1,D}}{\beta_{2,D}}\Big)^{1/2} \sum_{k=0}^{\infty} \delta_k \Big(\frac{R}{q_d P_t}\Big)^m \frac{{}_2F_1\Big(m, m+k+1; m+1; -\frac{R}{q_d P_t}\Big)}{mB(m,k+1)}}{\frac{\sigma_{\dot{g}}^2}{\sqrt{2\pi}} \sum_{D=1}^{D_{\max}} \mathbb{W}_D \Big(\frac{\beta_{1,D}}{\beta_{2,D}}\Big)^{1/2} \sum_{k=0}^{\infty} \delta_k \beta'(R; m, k+1, 1, \frac{P_t\Omega_{channel}}{m\beta_{1,D}})}$$

$$\text{CIN+AWGN: } \bar{t} = \frac{\sum_{A_c=0}^{A_{\max}} \mathbb{W}_{A_c,mca} \Big(\frac{\beta_{1,A_c}}{\beta_{2,A_c}}\Big)^{1/2} \sum_{k=0}^{\infty} \delta_k \Big(\frac{R}{q_d P_t}\Big)^m \frac{{}_2F_1\Big(m, m+k+1; m+1; -\frac{R}{q_d P_t}\Big)}{mB(m,k+1)}}{\frac{\sigma_{\dot{g}}^2}{\sqrt{2\pi}} \sum_{A_c=0}^{A_{\max}} \mathbb{W}_{A_c,mca} \Big(\frac{\beta_{1,A_c}}{\beta_{2,A_c}}\Big)^{1/2} \sum_{k=0}^{\infty} \delta_k \beta'(R; m, k+1, 1, \frac{P_t\Omega_{channel}}{m\beta_{1,A_c}})}$$

$$\begin{aligned}\text{CCI+CIN+AWGN: } \bar{t} = &\sum_{A_c=0}^{A_{\max}} \mathbb{W}_{A_c,mca} \sum_{D=1}^{D_{\max}} \mathbb{W}_D \sum_{k_1=0}^{\infty} \delta_{k_1} \Big(\frac{\beta_{1,D,A_c}}{\beta_{2,D,A_c}}\Big)^{1/2} \sum_{k_2=0}^{\infty} \delta_{k_2} \Big(\frac{\beta_{min}}{\beta_{\max}}\Big)^{k_1+1} \Big(\frac{R}{q_d P_t}\Big)^m \\ &\times \frac{{}_2F_1\Big(m, m+k_1+k_2+3/2; m+1; -\frac{R}{q_d P_t}\Big)}{mB(m, k_1+k_2+3/2)} \Big/ \Bigg\{ \frac{\sigma_{\dot{g}}^2}{\sqrt{2\pi}} \sum_{A_c=0}^{A_{\max}} \mathbb{W}_{A_c,mca} \sum_{D=1}^{D_{\max}} \mathbb{W}_D \sum_{k_1=0}^{\infty} \\ &\times \delta_{k_1} \Big(\frac{\beta_{1,D,A_c}}{\beta_{2,D,A_c}}\Big)^{\frac{1}{2}} \sum_{k_2=0}^{\infty} \delta_{k_2} \Big(\frac{\beta_{\min}}{\beta_{\max}}\Big)^{k_1+1} \beta' \left(R; m, k_1+k_2+3/2, 1, \frac{P_t\Omega_{channel}}{m\beta_{min}}\right) \Bigg\}.\end{aligned}$$

Remark 5. *If a particular state is defined as* $\mathbb{s}_i = \{\mathbb{s}_i \in (R_i, R_{i+1}) | R_i \in (R_i^-, R_i^+), R_i^+ - R_i^- \to \epsilon, \epsilon \to 0\}$, $\Delta R^i = R_{i+1}^- - R_i^+$ *is the span of the state, where* R_{i+1}^- *is the lower bound for the upper threshold and* R_i^+ *is the upper bound for the lower threshold. AFD is obtained as* $\bar{t}(R \in \Delta R^i) = \frac{\mathbb{F}(R_{i+1}) - \mathbb{F}(R_i)}{\eta_i}$, *where* $\mathbb{F}(\cdot)$ *is the CDF of the SPNR envelope. If the channel estimation is carried out at the receiver, the expression of AFD is modified as* $\bar{t}(R \in \Delta R^i) = \frac{1 - \mathbb{F}(R_i)/\mathbb{F}(R_{i+1})}{\eta_i}$.

C. Markov Model Formulation

1) Construction: The received SNR and SPNR range is divided into L sub-levels $[\gamma_0, \gamma_{L-1}]$ with each Markov state $\mathbb{s}_i$ confined between upper and lower thresholds such that $\mathbb{s} \in \{\mathbb{s}_1, \mathbb{s}_L\}$ and $\mathbb{s}_i \in (\gamma_{i-1}, \gamma_i]$. Let $\underline{\pi}$ denote a vector representing steady state probabilities for the $2L$ state Markov model in Fig. 2, where the first L states denote the channel state transition with successful

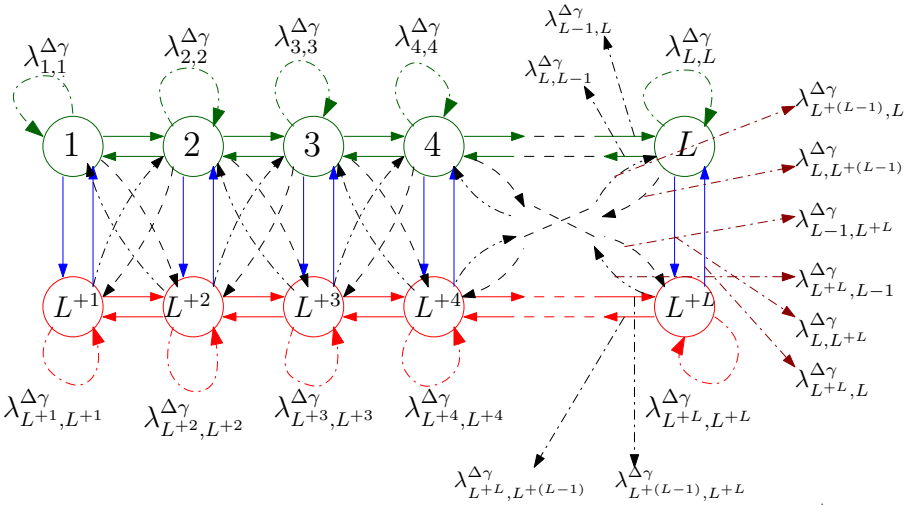

Fig. 2: Transition diagram of a $2L$ state Markov model for a Nakagami-m faded channel. L^{+n} : transmission failure state for n-th SPNR range ($\gamma_r^P \in (\gamma_{n-1}, \gamma]$). Lower(red): failed transmission, upper(green): successful transmission.

packet reception and last L states denote the channel transition under state of failure. The inter-level transitions occur when the channel renders a failed packet after a successful delivery in the previous slot, and vice-versa. It is assumed that the wireless channel is slowly fading, and hence there is no Markov chain state transition in the duration of a bit period. Additionally, under the same premise it can be inferred that only the transitions to adjacent states is possible.

A TCP connection is considered with fixed packet size $\mathscr{K}$. It can also be assumed without any loss of generality that the TCP transmission buffer always has a packet to transmit which is supported by the real time nature of the PMU data. At the beginning of the transmission the Markov chain starts at one of the upper L states with no bits in transmission. We will see later through Lemma 4 that this assumption can easily be relaxed keeping the analysis still intact as this doesn't affect the throughput values for a given SNR or SPNR. With the packet being transmitted the state transition will occur with the change in fading state of the channel. AMC is employed during transmission depending on the channel condition. Adaptive M-ary QAM and RS(c_i, k_i) channel coding is used and hence a packet is considered in error when the number of erroneous symbols in it exceed $(c_i - k_i)/2$ and the Markov chain will transit from one of the upper to the lower L states and then a retransmission for the same packet occurs when the transmitter does not receive an ACK bit from the receiver, therefore taking the Markov chain back to one of the upper L successful states, with a success for the resent packet.

Definition 1. *A Markov chain χ, defined on a finite state space $\mathbf{\Omega}$ with $|\Omega|^2$ dimension transition*

probability matrix $\boldsymbol{P}$ is s.t. $\mathbf{P}(X_{t+1} = y|X_t = x) = P(x, y)$ and a harmonic steady state vector $\underline{\pi} \in \boldsymbol{\Omega}$ with $\underline{\pi}\mathbf{P} = \underline{\pi}$ being the steady state equation for the Markov model.

Remark 6. *The SPNR is divided into L ranges s.t. state i refers to $\overline{\gamma} \in (\gamma_{i-1}, \gamma_i]$. Since every range of SPNR has the ability to both succeed or fail the packet delivery with a certain probability. Therefore every level bifurcates to two states, rendering either success or failure and thereby constituting the lower L failure states in the Markov model.*

2) Analysis: From the definition and construction it is noted that the Markov chain is irreducible i.e., $P^t(x, y) > 0$. Let the upper L states be from set $\mathscr{L}_u$ and lower L states set be $\mathscr{L}_l$. By Markov properties, the state transition probabilities $\lambda^{\Delta\gamma}_{m,n}$ from m to n ($\{m, n\} \in \mathbb{s}$) are [35]

$$\lambda^{\Delta\gamma}_{m,n} \approx \begin{cases} \mathscr{F}_i \frac{N_i}{R_t^{(i)}} & m = i \text{ or } L^{+i}, n = i + 1 \text{ and } i \in \{1, \cdots, L-1\} \\ \mathscr{F}_{i-1} \frac{N_{i-1}}{R_t^{(i)}} & m = i \text{ or } L^{+i}, n = i - 1 \text{ and } i \in \{2, \cdots, L\} \\ e_i \frac{N_i}{R_t^{(i)}} & m = i \text{ or } L^{+i}, n = L^{+(i+1)} \text{ and } i \in \{1, \cdots, L-1\} \\ e_{i-1} \frac{N_{i-1}}{R_t^{(i)}} & m = L^{+i}, n = L^{+(i-1)} \text{ and } i \in \{2, \cdots, L\} \end{cases} \tag{23}$$

where N^i is the expected number of downward crossings of the SNR/SPNR envelope through level γ_i, and $R_t^{(i)}$ is the average symbol transmission rate in state $\mathbb{s}_i$. e_i is the bit error probability in channel state $\mathbb{s}_i$ and $\mathscr{F}_i = 1 - e_i$. Remark 6 can be extended to state that $\lambda^{\Delta\gamma}_{w,L^{+w}} = \lambda^{\Delta\gamma}_{w,w}$ for some $w \in \mathbb{s}_i$, which follows from w and L^{+w} being defined on same SPNR ranges. Under the premise of steady state stability of the Markov chain, it can be formulated that,

$$\lambda^{\Delta\gamma}_{w,w} = \begin{cases} \mathscr{E}_w - \lambda^{\Delta\gamma}_{w,w+1} & , \text{ if } w = 1, L^{+1} \\ \mathscr{E}_w - \lambda^{\Delta\gamma}_{w,w-1} & , \text{ if } w = L, L^{+L} \\ \mathscr{E}_w - \lambda^{\Delta\gamma}_{w,w+1} - \lambda^{\Delta\gamma}_{w,w-1} & , \text{otherwise} \end{cases} \text{ with, } \mathscr{E}_w = \begin{cases} \mathscr{F}_w & w \in \mathscr{L}_u \\ e_w & w \in \mathscr{L}_l \end{cases}. \tag{24}$$

It is also worth noting that, since the time granularity of observation is much shorter compared to the channel fading time scale, only immediate state transitions are possible. Therefore, the transition probability matrix Ψ for the Markov model in Fig. 2 can be expressed as,

$$\Psi = \begin{bmatrix} \Psi_1 & \Psi_2 \\ \Psi_3 & \Psi_4 \end{bmatrix} \tag{25}$$

with Ψ_1 defined as the intra-good state transition probability matrix, Ψ_2 is the good to bad state transition probability matrix, Ψ_3 is the bad to good state transition probability matrix and Ψ_4 is the intra-bad state transition probability matrix. From Fig. 2 we can write,

$$\Psi_1 = \begin{bmatrix} \lambda_{1,1}^{\Delta\gamma} & \lambda_{1,2}^{\Delta\gamma} & 0 & \cdots & 0 \\ \lambda_{2,1}^{\Delta\gamma} & \lambda_{2,2}^{\Delta\gamma} & \lambda_{2,3}^{\Delta\gamma} & \cdots & 0 \\ 0 & \lambda_{3,2}^{\Delta\gamma} & \lambda_{3,3}^{\Delta\gamma} & \cdots & 0 \\ \vdots & \vdots & \vdots & \ddots & \vdots \\ 0 & 0 & 0 & \cdots & \lambda_{L,L}^{\Delta\gamma} \end{bmatrix}, \quad \Psi_2 = \begin{bmatrix} \lambda_{1,L^{+1}}^{\Delta\gamma} & \lambda_{1,L^{+2}}^{\Delta\gamma} & 0 & \cdots & 0 \\ \lambda_{2,L^{+1}}^{\Delta\gamma} & \lambda_{2,L^{+2}}^{\Delta\gamma} & \lambda_{2,L^{+3}}^{\Delta\gamma} & \cdots & 0 \\ 0 & \lambda_{3,L^{+2}}^{\Delta\gamma} & \lambda_{3,L^{+3}}^{\Delta\gamma} & \cdots & 0 \\ \vdots & \vdots & \vdots & \ddots & \vdots \\ 0 & 0 & 0 & \cdots & \lambda_{L,L^{+L}}^{\Delta\gamma} \end{bmatrix}$$

$$\Psi_3 = \begin{bmatrix} \lambda_{L^{+1},1}^{\Delta\gamma} & \lambda_{L^{+1},2}^{\Delta\gamma} & 0 & \cdots & 0 \\ \lambda_{L^{+2},1}^{\Delta\gamma} & \lambda_{L^{+2},2}^{\Delta\gamma} & \lambda_{L^{+2},3}^{\Delta\gamma} & \cdots & 0 \\ 0 & \lambda_{L^{+3},2}^{\Delta\gamma} & \lambda_{L^{+3},3}^{\Delta\gamma} & \cdots & 0 \\ \vdots & \vdots & \vdots & \ddots & \vdots \\ 0 & 0 & 0 & \cdots & \lambda_{L^{+L},L}^{\Delta\gamma} \end{bmatrix}, \Psi_4 = \begin{bmatrix} \lambda_{L^{+1},L^{+1}}^{\Delta\gamma} & \lambda_{L^{+1},L^{+2}}^{\Delta\gamma} & 0 & \cdots & 0 \\ \lambda_{L^{+2},L^{+1}}^{\Delta\gamma} & \lambda_{L^{+2},L^{+2}}^{\Delta\gamma} & \lambda_{L^{+2},L^{+3}}^{\Delta\gamma} & \cdots & 0 \\ 0 & \lambda_{L^{+3},L^{+2}}^{\Delta\gamma} & \lambda_{L^{+3},L^{+3}}^{\Delta\gamma} & \cdots & 0 \\ \vdots & \vdots & \vdots & \ddots & \vdots \\ 0 & 0 & 0 & \cdots & \lambda_{L^{+L},L^{+L}}^{\Delta\gamma} \end{bmatrix}.$$

Remark 7. *From state $\mathscr{N}$ of the Markov chain, the possible transitions are $\mathscr{N}+1$, $\mathscr{N}-1$, $\mathscr{N}$, $L^{+\mathscr{N}}$, $L^{+(\mathscr{N}+1)}$, and $L^{+(\mathscr{N}-1)}$. Using the transition probability definition in* (23) *and* (24)*, the probability of leaving state $\mathscr{N}$ sums up to 1, which proves statistical stability of the chain.*

Let the packet transmission start with the channel state j, such that $j \in \mathbb{s}$. The channel state indicator array $\mathscr{I}_j$ for state j can be defined as: $\mathscr{I}_j = [0_1, \cdots, 0_{j-1}, 1, 0_{j+1}, \cdots, 0_{2L}]$, with 0_j being the zero in the j-th position in the indicator array. Thus, the transition probability matrix $\mathbf{P}$ for the Markov model can be expressed as: $\mathbf{P} = [\mathscr{I}_1^T, \mathscr{I}_2^T, \cdots, \mathscr{I}_{2L}^T]^T \Psi^{\mathscr{K}}$, with $\mathscr{K}$ bytes in transit. The steady state probability vector $\underline{\pi}$ can be obtained using $\underline{\pi} = \underline{\pi}\mathbf{P}$.

Lemma 4. *The average throughput for a given received SPNR or SNR is independent of the knowledge of initial channel state when the data transmission started.*

Algorithm 1: Calculation of average throughput T_p

Result: Throughput T_p for different received power
Initialize $\mathscr{K}$ = TCP packet size and T_p with all zeros
for $\gamma_{Received} = \gamma_{min} \rightarrow \gamma_{\max}$ **do**
  Initialize vector $\mathbb{I}_{states}$ and $\mathbf{P}$ at initial zeros
  for *states* $= 1 \rightarrow 2L$ **do**
    $\mathscr{I}(states) = 0$
    N^{states} = LCR through level '$l = states$'
    e_{states} = bit error probability with and without AMC
    $\mathbf{P}(states, :) = \mathscr{I}_{states} * \Psi^{\mathscr{K}}$
  end
  Calculate throughput T_p for different values of received SPNR $\overline{\gamma}$
end

Proof. See Appendix C. □

$\underline{\pi}$ is calculated by Algorithm 1. Further, using Lemma 4, network throughput is obtained as,

$$T_p = \sum_{i=1}^{L} \underline{\pi}_i$$

which is the sum of the steady state probabilities for the upper L successful states.

VI. Results and Discussions

This section presents a numerical evaluation of the analysis done in the previous sections. The simulation parameters used are listed in Table II, where γ_{th} values for 'no signal', 'fair to poor', 'good' and 'excellent' levels are based on the LTE specifications. We use $P_t = 100$ mW, $d \in (d_{min}, d_{\max})$ with $d_{min} = 100$ m to $d_{\max} = 1$ Km, $\lambda_s \in (1, 5)$ sec^{-1}, and $\lambda_\alpha \in (5, 1000)$ sec^{-1} with the lower extreme denoting normal and the upper extreme of the range denoting an extreme day. Path-loss exponent values are $\eta \in [2, 4]$. The TCP packet size of $\mathscr{K} = 576$ bytes is considered. We use the approximation $m = \frac{k^2+2k+1}{2k+1}$, where m is the shape parameter of Nakagami-m distribution and k is the $k-$factor of Rice distribution in outage analysis. Also, all the corona noise intensity values used in motivating as well as analyzing the effects of EMN are as per the standards defined in IS: 5613-1-1 (1985) and AS/NZS 7000 guidelines.

A. CIN Model Validation

As the statistical nature of the source distribution changes (identical or non-identical), the weight functions change, which is intuitive based on the statistical contribution that they would

TABLE II: Simulation parameters used in throughput analysis using Markov model

	Mode-1	Mode-2	Mode-3	Mode-4
γ_{th} (dB)	< 0	$0 - 13$	$13 - 20$	> 20
Modulation	BPSK	QPSK	16$-$QAM	64$-$QAM
Code rate (k/n)	$1/2$	$1/2$	$3/4$	$3/4$
P_t (in mW)	500	400	200	100

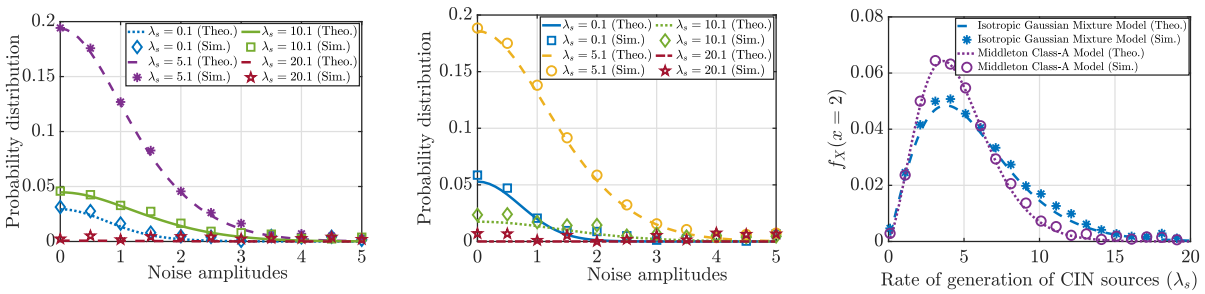

(a) (b) (c)

Fig. 3: Probability distribution for (a) isotropic Gaussian mixture model, (b) Middleton class-A model, with the different rate of CIS generation λ_s (c) probability of generation of 2 CIN sources versus rate of generation of CIN sources for isotropic Gaussian mixture and Middleton class-A model. Theo.: theoretical plot; Sim.: simulation plot

render in the total distribution. For example, if the sources are identical, the model turning out to be weighed in an isotropic manner as shown in Fig. 3(a) is quite realistic, as the Euclidean norm between the impulse generating sources and the receiver is more significant as opposed to the direction of their presence. To simplify, the impact at a receiver placed at $\vec{x_r}$ from a CIN source located at $\vec{x_t}$ is dependent on $||\vec{x_r} - \vec{x_t}||$ and not on $\vec{x_r} - \vec{x_t}$, which is basically due to the sources being statistically identically distributed. When the assumption of identical source distribution is relaxed, the mixture components now become Poisson weighed, which can be defended from the experimentally verified distributions for electromagnetic interference proposed in [36] and is shown in Fig. 3(b). The Gaussian mixture manifestation can be seen to be aided from the central limit theorem owing to the large number of impulse emissions from CISs.

Validation of derived CIN density models is done in Fig. 3. The plots in Fig. 3(a) and Fig. 3(b) capture the CIN amplitude distribution at various source generation intensities λ_s for an isotropic Gaussian mixture model and Middleton class-A model respectively. A good overlap between theoretical and Monte-Carlo simulation plots validate the analytical expressions in (7) and (11). Further, Fig. 3(c) gives an idea about the variation of the proposed density models with λ_s, where the Monte-Carlo simulation again corresponds with the theoretical results.

B. Outage Probability

The variation of outage probability for different values of received SPNR is shown in Fig. 4(a). From the plot, it is evident that a channel having the impact of corona noise behaves poorer than the one with CCI. From the result in Fig. 4(b), it can be inferred that even with dense CCI in the smart grid environment, the outage probability for a CIN ridden channel is poor. A CCI environment is worse only at magnitudes $2-3$ times stronger as compared to CIN which is positively correlated with the fading margin. The CuRD index, which is an affine sum of ratio of variance to mean for wanted power to unwanted power in a mixture model, gives a strong conclusion on the nature of a noise. The normalized variation of CuRD index q_d against $\overline{\gamma}$ is shown in (a). As this value tends to 1, the effect of the noise on the data becomes more bursty, thereby decreasing the data success probability. Therefore, though the outage probability for CCI and CIN ridden channels might overlap or even crossover in dense CCI scenarios, CuRD index gap for these cases is quite high and therefore CIN is always a worse noise to encounter. The plot in Fig. 4(c) further strengthens this claim by addressing the variation of outage probability with γ_{th}. From the plots, it can be seen that the outage with corona noise always supersedes all other noise scenarios discussed. The variation of outage probability with the relative strength of LOS component I_{los} is studied in Fig.4(d). As the strength of the LOS component enhances, the success rate increases for all noise profiles with corona noise still being the worse impulsive noise. Also, as the fading margin decreases, the outage probability with CIN increases for the same $\overline{\gamma}$, which is a direct conclusion that can be drawn here. Further, we verify the sanity of derived analytical forms using Monte-Carlo simulation as shown through marker curves in Fig. 4. The plots for the outage probability variations shown in Fig. 4(a)-(d) show a nice overlap between simulation (represented by markers) and derived analytical forms (represented by different line types). This strong correspondence between analytical and simulation results conclude the correctness of the outage mathematical analysis presented in the paper.

Remark 8. *A trade-off between CuRD index and outage probability can be noted from the analysis. While bit error rate can be reduced by increased SPNR, CuRD index plots indicate that this will also increase the chances of more bits being in error.*

Remark 9. *The performance of a CIN impaired wireless communication is always poorer because of its tendency to collate the data points away from the mean value. Intuitively, this*

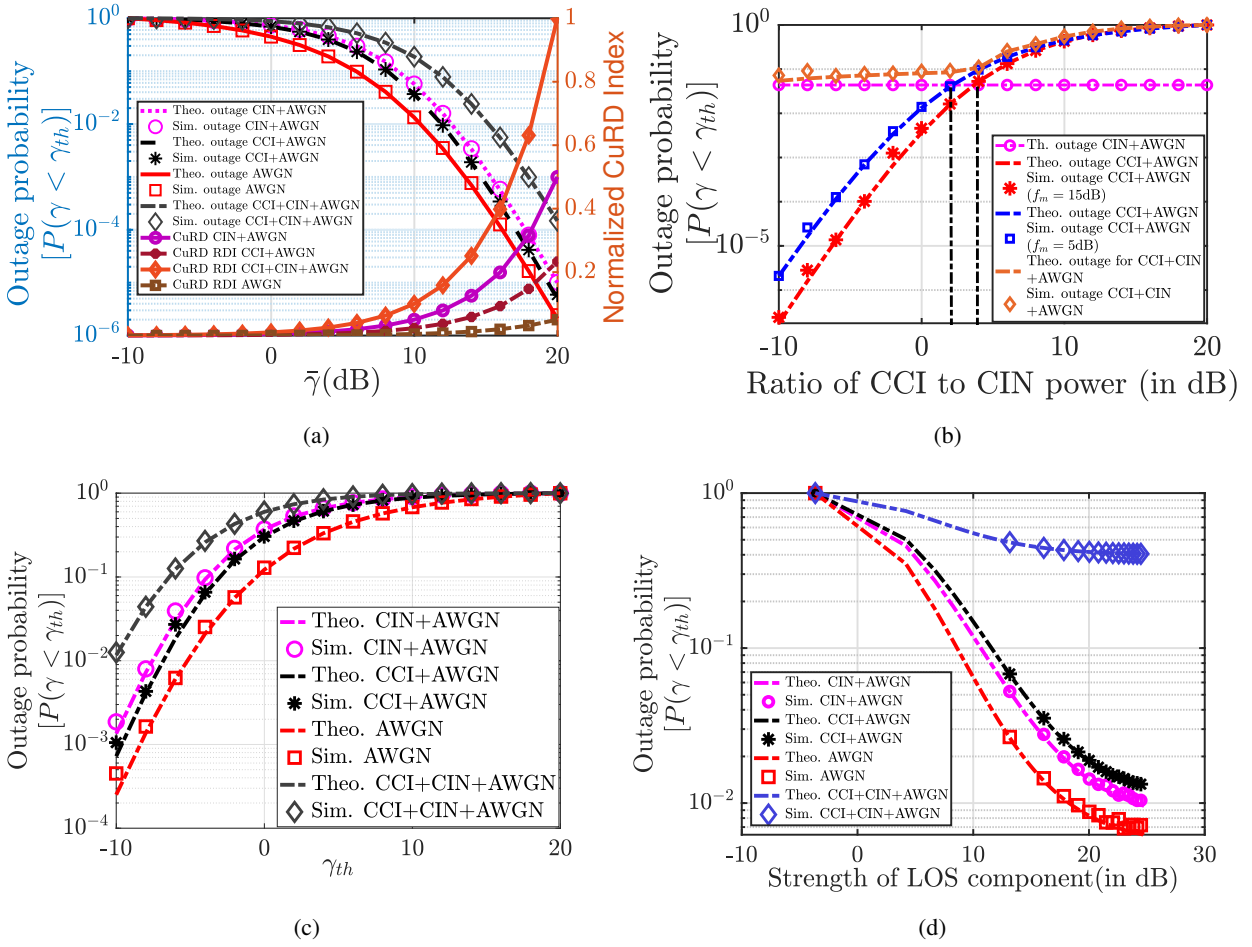

Fig. 4: (a) Variation of outage probability and CuRD Index with $\overline{\gamma}$ (b) variation of outage probability with CCI power relative to CIN (in dB), at $\gamma_{th} = 5$ dB and $\overline{\gamma} = 6$ dB (c) variation of outage probability with γ_{th} (d) variation of outage probability with relative strength of line-of-sight component at $f_m = 5$ dB.

would mean that the noise sources are highly impulsive and random in space and time, which also supports the claim on inadequacy of the average SPNR modeling.

C. Average Throughput

The average throughput over the Nakagami-m channel under different noise profiles are plotted in Figs. 5(a) and 5(b) against the average received SPNR, respectively with power control and with AMC, using the parameters in Table II. It can be observed that the average throughput over the CIN ridden channel is always poorer as compared to that with CCI. To combat CIN, more transmit power or more coding overhead is needed in worse SPNR ranges to counter more interference. It is further noted that the maximum average throughput (≈ 0.77 from Fig. 5(a)) for the best case AWGN channel with power control is closer to the maximum average throughput

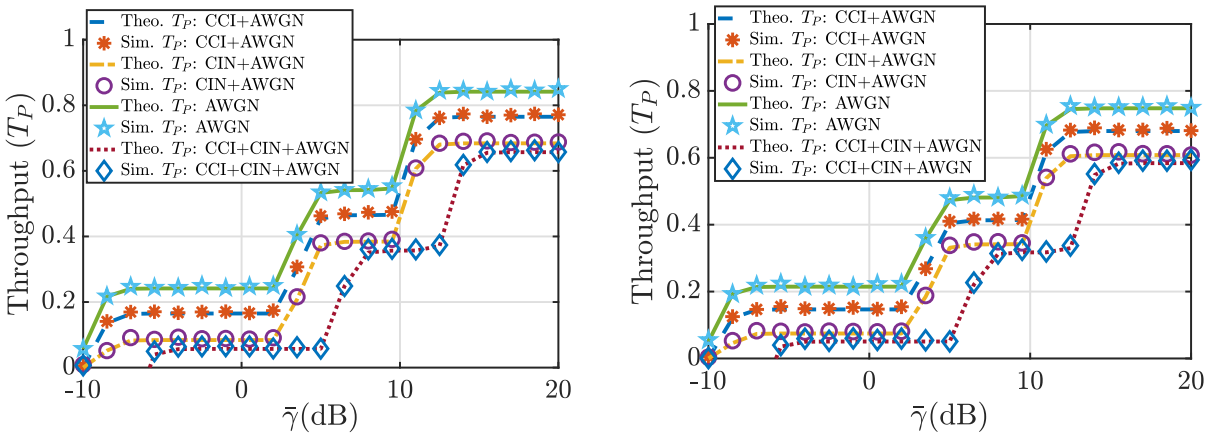

Fig. 5: Variation of average throughput T_p with $\overline{\gamma}$ for a Nakagami-m faded channel (a) with power control (b) with AMC without power control at $P_t = 100$ mW.

($\approx$ 0.7 from Fig. 5(b)) for the CIN impaired channel with AMC. This gives a fair idea on the transmission strategy including AMC overheads and transmit power to be used in wireless communication through electromagnetic impulse noise environments. From the comparative study of the plots it can be noted that transmitting at lower power with higher coding overheads can achieve better throughput. Also, we undertook Monte-Carlo simulation technique to verify the throughput analytical formulations. The close correspondence of the simulation plots with theoretical plots as is seen in Fig. 5 verify the correctness of the derived formulations.

VII. Concluding Remarks

In this paper, the performance of a Nakagami-m faded wireless communication channel in presence of CIN, which is an EMN has been investigated and compared with pre-established CCI. This power system specific EMN modeling in smart grid wireless communication is found to represent a Middleton class-A model and isotropic Gaussian mixture model under two different simplified scenarios. The derived exact expressions for total unwanted noise power, SPNR, and SNR for the four proposed noise profiles give a strong modeling insight. The derived exact forms reduce to closed-form expressions for all practical purposes because the number of summands is limited to a finite number. It can be observed that the dimensionality of the models, can be addressed through the '$\sum$' operator prefixed to them with appropriate weights. The CIN analysis has addressed randomness of both the number of sources and impulses per source. The variation of outage probability with $\overline{\gamma}$, γ_{th}, and LOS strength has been mathematically

analyzed and numerically simulated, to establish the impact of corona noise on smart grid wireless communication. Exact expressions for the LCR and AFD for all the noise profiles have been derived to analyze the Markov model formulated using the channel states defined on SPNR thresholds according to LTE specifications. The throughput with power control and AMC has also been investigated separately. The analysis shows that a CIN impaired wireless communication channel always performs poorer. The BER and throughput study in this paper asserts that the CIN needs to be appropriately accounted for effective communication of time-critical IoT data in smart grid environment.

APPENDIX

A. *Proof of Lemma* 2

Let Y (received signal power) be a gamma distributed random variable, and define $X = X_1 + X_2 + \cdots + X_N$ where X_is are mutually independent gamma distributed random variables. Then using Theorem 1 of [32], the distribution of X (total unwanted power) can be derived as a gamma mixture model. Therefore, using the idea of ratio distribution, we have $Z = Y/X$ as

$$f_Z(z) = \int_{-\infty}^{\infty} |y| f_Y(zy) f_X(y) dy \tag{A1}$$

where $f_X(x)$ and $f_Y(y)$ are the density functions of random variables X and Y respectively. For brevity, we now drop the subscript Z from $f_Z(z)$. Further, following Lemma 1 for the distribution of X and using it to derive the distribution of Z (received SPNR) through (A1), we have

$$f(z) = \int_0^{\infty} z^{m-1} \frac{m^m}{\Gamma(m)\Omega^m} \sum_{i=1}^{N} \omega_i \Big(\frac{\beta_{1,i}}{\beta_{2,i}}\Big)^{1/2} \sum_{k=0}^{\infty} \frac{\delta_k}{k!\beta_{1,i}^{k+1}} y^{k+m} e^{\frac{-y}{\beta_{1,i}} + \frac{-mzy}{\Omega}} dy. \tag{A2}$$

Define $h_i^{\mathbb{1}}(y) = \omega_i \Big(\frac{\beta_{1,i}}{\beta_{2,i}}\Big)^{\frac{1}{2}} \sum_{k=0}^{\infty} \frac{\delta_k}{k!\beta_{1,i}^{k+1}} y^{k+m} e^{\frac{-y}{\beta_{1,i}} + \frac{-myz}{\Omega}}$. It can be observed that $h_i^{\mathbb{1}}(y)$ is strictly positive $\forall i$ and $y \in \mathbb{R}^+$. Therefore, using Tonelli's theorem, the integration in (A2) can be taken inside the summation over i. Again applying Tonelli's theorem on $h_i^2(y) = \frac{\delta_k}{k!\beta_{1,i}^{k+1}} y^{k+m} e^{\frac{-y}{\beta_{1,i}} + \frac{-myz}{\Omega}}$, the integration can be moved even through the second summation on k in (A2).

$$f(z) = z^{m-1} \frac{m^m}{\Gamma(m)\Omega^m} \sum_{i=1}^{N} \omega_i \Big(\frac{\beta_{1,i}}{\beta_{2,i}}\Big)^{1/2} \sum_{k=0}^{\infty} \frac{\delta_k}{k!\beta_{1,i}^{k+1}} \int_0^{\infty} y^{k+m} e^{\frac{-y}{\beta_{1,i}} + \frac{-myz}{\Omega}} dy. \tag{A3}$$

Integrating the N summands term-wise and by the principle of mathematical induction, we get

$$f(z) = \sum_{i=1}^{N} \omega_i \Big(\frac{\beta_{1,i}}{\beta_{2,i}}\Big)^{1/2} \sum_{k=0}^{\infty} \delta_k \frac{\Big(\frac{z}{\Omega/m\beta_{1,i}}\Big)^{m-1} \Big(1+\frac{z}{\Omega/m\beta_{1,i}}\Big)^{-m-k-1}}{(\Omega/m\beta_{1,i})B(m,k+1)}$$
$$= \sum_{i=1}^{N} \omega_i \Big(\frac{\beta_{1,i}}{\beta_{2,i}}\Big)^{1/2} \sum_{k=0}^{\infty} \delta_k \beta'\Big(z; m, k+1, 1, \frac{\Omega}{m\beta_{1,i}}\Big)$$

where ω_i is the weight of i-th mixture component in x, $\beta_1 = min(\mathbb{E}[(x_1-\mu_{x_1})^2], \mathbb{E}[(x_2-\mu_{x_2})^2], \cdots, \mathbb{E}[(x_N-\mu_{x_N})^2])$ and $\beta_2 = \max(\mathbb{E}[(x_1-\mu_{x_1})^2], \mathbb{E}[(x_2-\mu_{x_2})^2], ..., \mathbb{E}[(x_N-\mu_{x_N})^2])$ for the i-th mixture component. Thus, Z distribution follows beta prime mixture model.

B. Proof of Lemma 3

As the channel fading envelope x is considered Nakagami-m distributed, therefore,

$$f(x) = \frac{2m^m}{\Gamma(m)\Omega^m} x^{2m-1} \exp\Big(-\frac{m}{\Omega}x^2\Big)$$

and therefore the distribution of $y = x^2$ may be given as,

$$f(y) = \frac{m^m}{\Gamma(m)\Omega^m} y^{m-1} \exp\Big(-\frac{m}{\Omega}y\Big) = \mathbb{\Gamma}\Big(y; m, \frac{m}{\Omega}\Big). \tag{B1}$$

Now, using central limit theorem any highly impulsive noise or interference can always be modeled as a Gaussian mixture model (alternate proof in Section III-A), and hence the square of this random variable is a gamma mixture model. In presence of receiver thermal noise, using Lemma 1, the total unwanted power z can be modeled as a gamma mixture model.

Therefore using Lemma 2, the ratio of these random variables, $g \overset{(def)}{=} \frac{Y}{Z}$ is modeled as a beta prime mixture model. From the result in [37], we know that $\mathbb{E}[(G-\mathbb{E}(G))(\dot{G}-\mathbb{E}(\dot{G}))] = 0$ and $\dot{g}$ follows a normal distribution. Using the definition of LCR, we have,

$$LCR(:=\eta) = \int_0^{\infty} \dot{g} f_{G\dot{G}}(g,\dot{g}) d\dot{g}\Big|_{g=R} = \Big(\int_0^{\infty} \dot{g} f_{\dot{G}}(\dot{g}) d\dot{g}\Big) f_G(g)\Big|_{g=R} = \frac{\sigma_{\dot{g}}^2}{\sqrt{2\pi}} f_G(R) \tag{B2}$$

where $\sigma_{\dot{g}}^2$ is the variance of the derivative distribution of g, and $f_G(R)$ is the density function of G. It can be inferred from (B2) that the expression for LCR of a Nakagami-m channel in a highly impulsive environment is a scaled version of the distribution of g.

C. Proof of Lemma 4

Let the Markov chain χ be irreducible ($P^t(x,y) > 0$) with the state transition probability matrix $\mathbf{P}$ and stationary distribution $\underline{\pi}$ such that $\underline{\pi} = \underline{\pi}\mathbf{P}$ with $|\underline{\pi}| = \Omega$ (from Def. 1).

Now let $\underline{h}$ be a harmonic vector on set Ω such that h attains a maximum at some arbitrary state $x_0 \in \Omega$. Therefore, $h(x_0) > h(r)\ \forall r \in \Omega$. Let us assume a state $z \in \Omega$ s.t. $P(x_0, z) > 0$ and consider $h(z) - h(x_0) < 0$. Since h is harmonic at x_0, we have,

$$\begin{aligned} h(x_0) &= \sum_{r\in\Omega} P(x_0,r)h(r) = P(x_0,z)h(z) + \sum_{r\in\Omega, r\neq z} P(x_0,r)h(r) \\ &\leq P(x_0,z)h(z) + \sum_{r\in\Omega, r\neq z} P(x_0,r)h(x_0) \leq P(x_0,z)h(x_0) + \sum_{r\in\Omega, r\neq z} P(x_0,r)h(x_0) \\ &= \left(\sum_{r\in\Omega} P(x_0,r)\right) h(x_0) = h(x_0). \end{aligned}$$

Thus, we have $h(x_0) < h(x_0)$, which is a contradiction. Hence, $h(x_0) = h(r)$, implying that $\underline{h}$ is a stationary distribution. Accordingly, we have $h(x) = c\ \forall x \in \Omega$. In vector notation this results in $Ph = h$ or equivalently $(\mathbf{P} - \mathbf{I})\underline{h} = \underline{0}$ with $\underline{h}^T = c[1, 1, \cdots, 1]$ as the family of solutions. Thus, $dim(ker(\mathbf{P} - \mathbf{I})) = 1$. By rank-nullity theorem rank$(\mathbf{P} - \mathbf{I}) = |\Omega| - 1$. We therefore have,

$$rank(\mathbf{P} - \mathbf{I}) = rank(\mathbf{P} - \mathbf{I})^T = rank(\mathbf{P}^T - \mathbf{I}) = |\Omega| - 1 \tag{26}$$

Again by rank-nullity theorem $dim(ker(\mathbf{P}^T - \mathbf{I})) = 1$. Therefore, over all row vectors $\underline{v} \in \mathbb{R}^{|\Omega|}$, $(\mathbf{P}^T - \mathbf{I})\underline{v} = 0$ has only a one-dimensional space of solutions. But this is equivalent to $\mathbf{P}\underline{v} = \underline{v}$. Given that $\mathbf{P}\underline{\pi} = \underline{\pi}$ is a solution from the initial assumption, we know that the family of solutions must be of the form $\underline{v} = k\underline{\pi}$. However, for $\underline{v}$ to be a valid probability distribution, $k = 1$. Therefore, $\underline{v} = \underline{\pi}$ is a unique and stationary distribution. As average throughput is defined as packet success rate in this work, we have $throughput = \sum_{i=1}^{|\Omega|/2} \underline{\pi}_i$, which is independent of the initial channel state information owing to the uniqueness and stationarity proven for $\underline{\pi}$.

REFERENCES

[1] S. Dasgupta, M. Paramasivam, U. Vaidya, and V. Ajjarapu, "Real-Time Monitoring of Short-Term Voltage Stability Using PMU Data," *IEEE Trans. Power Syst.*, vol. 28, no. 4, pp. 3702–3711, 2013.

[2] M. Biswal, S. M. Brahma, and H. Cao, "Supervisory Protection and Automated Event Diagnosis Using PMU Data," *IEEE Trans. Power Del.*, vol. 31, no. 4, pp. 1855–1863, 2016.

[3] W. Pakala and V. Chartier, "Radio noise measurements on overhead power lines from 2.4 to 800 kV," *IEEE Trans. Power App. Syst.*, no. 3, pp. 1155–1165, 1971.

[4] S. Niranjayan and N. C. Beaulieu, "Analysis of wireless communication systems in the presence of non-Gaussian impulsive noise and Gaussian noise," in *Proc. IEEE Wireless Commun. Netw. Conf.,*, 2010, pp. 1–6, Sydney, NSW, Australia.

[5] D. Moongilan, "Corona noise considerations for smart grid wireless communication and control network planning," in *Proc. IEEE Int. Symp. Electromagn. Compat.*, 2012, pp. 357–362, Pittsburgh, PA, USA.

[6] F. Sacuto, F. Labeau, and B. L. Agba, "Wide band time-correlated model for wireless communications under impulsive noise within power substation," *IEEE Trans. Wireless Commun.*, vol. 13, no. 3, pp. 1449–1461, 2014.

[7] M. Tanaka, "High frequency noise power spectrum, impedance and transmission loss of power line in japan on intrabuilding power line communications," *IEEE Trans. Consum. Electron.*, vol. 34, no. 2, pp. 321–326, 1988.

[8] D. Moongilan., "Corona and arcing in power and RF devices," in *IEEE Symp. Product Compliance Engineering*, 2009, pp. 1–7.

[9] G. Ndo, F. Labeau, and M. Kassouf, "A Markov-Middleton model for bursty impulsive noise: Modeling and receiver design," *IEEE Trans. Power Del.*, vol. 28, no. 4, pp. 2317–2325, 2013.

[10] M. Nassar, K. Gulati, Y. Mortazavi, and B. L. Evans, "Statistical modeling of asynchronous impulsive noise in powerline communication networks," in *Proc. IEEE Global Commun. Conf.*, 2011, pp. 1–6, Houston, TX, USA.

[11] D. Middleton, "Statistical-physical models of electromagnetic interference," *IEEE Trans. Electromagn. Compat.,*, no. 3, pp. 106–127, 1977.

[12] N. B. Rached, A. Kammoun, M.-S. Alouini, and R. Tempone, "A unified moment-based approach for the evaluation of the outage probability with noise and interference," *IEEE Trans. Wireless Commun.*, vol. 16, no. 2, pp. 1012–1023, 2016.

[13] A. G. Lazaropoulos and P. G. Cottis, "Capacity of overhead medium voltage power line communication channels," *IEEE Trans. Power Del.*, vol. 25, no. 2, pp. 723–733, 2009.

[14] K. M. Rabie and E. Alsusae, "On Improving Communication Robustness in PLC Systems for More Reliable Smart Grid Applications," *IEEE Trans. Smart Grid*, vol. 6, no. 6, pp. 2746–2756, 2015.

[15] N. Suljanovic, A. Mujcic, M. Zajc, and J. F. Tasic, "Computation of high-frequency and time characteristics of corona noise on HV powerline," *IEEE Trans. Power Del.*, vol. 20, no. 1, pp. 71–79, 2005.

[16] F.-C. Lu, S.-H. You, Y.-P. Liu, Q.-F. Wan, and Z.-B. Zhao, "AC Conductors' Corona-Loss Calculation and Analysis in Corona Cage," *IEEE Trans. Power Del.*, vol. 27, no. 2, pp. 877–885, 2012.

[17] Q. Li, S. M. Rowland, I. Dupere, and R. Shuttleworth, "Acoustic Noise Evaluation for Overhead Line Conductors Using an Anechoic Chamber," *IEEE Trans. Power Del.*, vol. 32, no. 4, pp. 1835–1843, 2017.

[18] M. Antoniali, F. Versolatto, and A. M. Tonello, "An Experimental Characterization of the PLC Noise at the Source," *IEEE Trans. Power Del.*, vol. 31, no. 3, pp. 1068–1075, 2016.

[19] A. Mujčić, N. Suljanović, M. Zajc, and J. Tasič, "Corona noise on a 400 kV overhead power line: Measurements and computer modeling," *Electrical engineering*, vol. 86, no. 2, pp. 61–67, 2004.

[20] A. Shojaeifard, K. A. Hamdi, E. Alsusa, D. K. So, and J. Tang, "Exact SINR statistics in the presence of heterogeneous interferers," *IEEE Trans. Inf. Theory*, vol. 61, no. 12, pp. 6759–6773, 2015.

[21] F. Kalbat, A. Al-Dweik, B. Sharif, and G. K. Karagiannidis, "Performance analysis of precoded wireless OFDM with carrier frequency offset," *IEEE Syst. J.*, 2019.

[22] F. A. Asuhaimi, S. Bu, P. V. Klaine, and M. A. Imran, "Channel access and power control for energy-efficient delay-aware heterogeneous cellular networks for smart grid communications using deep reinforcement learning," *IEEE Access*, vol. 7, pp. 133 474–133 484, 2019.

[23] K. A. Hamdi, "Exact SINR analysis of wireless OFDM in the presence of carrier frequency offset," *IEEE Trans. Wireless Commun.*, vol. 9, no. 3, pp. 975–979, 2010.

[24] M. Ahsen and S. A. Hassan, "On the ratio of exponential and generalized gamma random variables with applications to ad hoc SISO networks," in *Proc. IEEE Veh. Technol. Conf.*, 2016, pp. 1–5, Montreal, QC.

[25] A. Kudeshia, A. K. Jagannatham, and L. Hanzo, "Total Variation Based Joint Detection and State Estimation for Wireless Communication in Smart Grids," *IEEE Access*, vol. 7, pp. 31 598–31 614, 2019.

[26] J. I. Huertas, R. Barraza, and J. M. Echeverry, "Wireless data transmission from inside electromagnetic fields," in *Proc. IEEE 11th Electric Power Conf.*, 2009, pp. 1–7, Toluca, Mexico.

[27] P. S. Maruvada, *Corona performance of high-voltage transmission lines*. Research Studies Press Baldock, Herfordshire, United Kingdom, 2000.

[28] H. H. Farr, *Transmission line design manual*. US Department of the Interior, Water and Power Resources Service, 1980.

[29] T. Johnson and T. Moger, "A critical review of methods for optimal placement of phasor measurement units," *Int. Trans. Electr. Energy Syst.*, p. e12698, 2020.

[30] A. Shojaeifard, K. A. Hamdi, E. Alsusa, D. K. C. So, J. Tang, and K.-K. Wong, "Design, Modeling, and Performance Analysis of Multi-Antenna Heterogeneous Cellular Networks," *IEEE Trans. on Commun.*, vol. 64, no. 7, pp. 3104–3118, 2016.

[31] D. Middleton, "Procedures for determining the parameters of the first-order canonical models of Class A and Class B electromagnetic interference," *IEEE Trans. Electromagn. Compat.*, no. 3, pp. 190–208, 1979.

[32] P. G. Moschopoulos, "The distribution of the sum of independent gamma random variables," *Ann. Inst. Statist. Math. (Part A)*, vol. 37, no. 3, pp. 541–544, 1985.

[33] A. Abdi, K. Wills, H. A. Barger, M.-S. Alouini, and M. Kaveh, "Comparison of the level crossing rate and average fade duration of Rayleigh, Rice and Nakagami fading models with mobile channel data," in *Proc. IEEE Veh. Technol. Conf.*, vol. 4, 2000, pp. 1850–1857, Boston, MA, USA.

[34] Z. Hadzi-Velkov, "Level crossing rate and average fade duration of EGC systems with co-channel interference in Rayleigh fading," *IEEE Trans. Commun.*, vol. 55, no. 11, pp. 2104–2113, 2007.

[35] H. S. Wang and N. Moayeri, "Finite-state Markov channel-a useful model for radio communication channels," *IEEE Trans. Veh. Technol.*, vol. 44, no. 1, pp. 163–171, 1995.

[36] D. Middleton, "Statistical-Physical Models of Electromagnetic Interference," *IEEE Trans. Electromagn. Compat.*, vol. EMC-19, no. 3, pp. 106–127, 1977.

[37] S. L. Cotton, "Second-Order Statistics of $\kappa - \mu$ Shadowed Fading Channels," *IEEE Trans. Veh. Technol.*, vol. 65, no. 10, pp. 8715–8720, 2015.